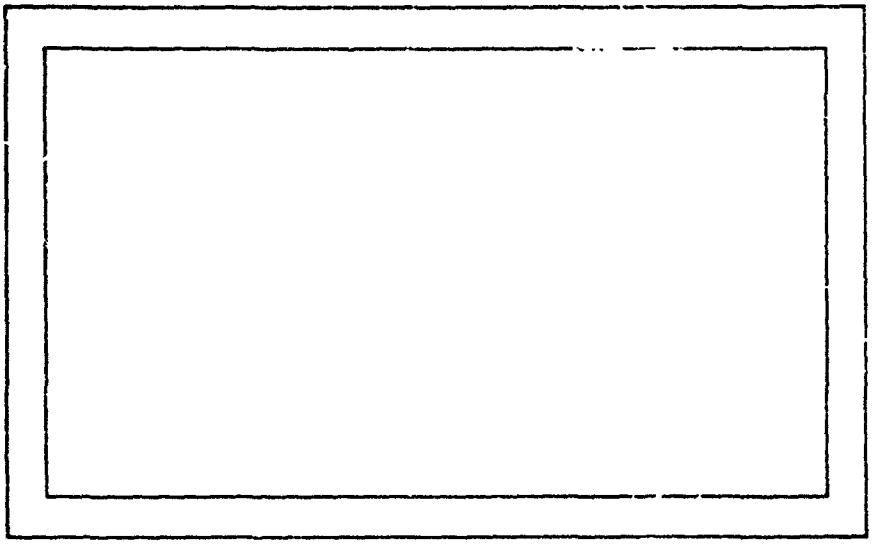

THERM ADVANCED RESEARCH
DIVISION OF
THERM
ITHACA NEW YORK

THREE-DIMENSIONAL THEORY

OF

DUCTED PROPELLERS

by

D.E. Ordway, M.M. Sluyter, B.O.U. Sonnerup

TAR-TR 602 August 1960

Submitted to the Air Branch, Office of
Naval Research in partial fulfillment of
Contract Nonr-2859(00)

Donald Earl Ordway
Donald Earl Ordway
Head, Aerophysics Section

Approved: A. Ritter
A. Ritter
Director
Therm Advanced Research

ACKNOWLEDGMENT

The authors wish to express their sincere appreciation to Dr. H. S. Tan, Dr. A. Ritter and to Dr. D. A. Spence for their many suggestions and discussions; to Michael Greenberg for his thorough review of the manuscript and computations of the numerical example; and to Barbara Elliott and Lynn Warren for their wonderful assistance in final report preparation.

The authors also wish to acknowledge the interest, enthusiasm and fine project coordination of Dr. G. B. Matthews and LCDR A. Van Tuyl of the Office of Naval Research.

ABSTRACT

This study treats the ducted propeller with finite blade number at zero angle of attack in a uniform, incompressible, inviscid flow. The approximations of a lightly loaded propeller and of thin airfoil theory are made. In the absence of thickness effects, appropriate vortex distributions represent the blades, the shroud and their respective shed vortices. By means of Fourier analysis of the velocity field in propeller fixed coordinates, the problem for an arbitrary, radial blade circulation distribution is reduced to a form similar to the ring wing integral equations of J. Weissinger. The kernels are not the same for the two cases except for the zeroth harmonic. The equation for this harmonic, which corresponds to a generalized actuator disk formulation, is identical to that of an equivalent, axisymmetric ring wing. The effect of blade number, blade circulation profile and strength, propeller advance ratio and tip clearance, and location of the propeller plane are found and may be evaluated over a range of parameters from tables provided. A numerical example is given.

TABLE OF CONTENTS

NOMENCLATURE

A_m, ...	amplitudes of sine term of Fourier harmonic
B_m, ...	amplitudes of cosine term of Fourier harmonic
C_m, ...	amplitudes of complex Fourier harmonic
D	distance between vortex element and field point
$F_{\gamma m}$, ...	functions of complex kernel of intermediate form of governing equations
$G_n(\kappa^2)$	Riegels function
I_h, I_p, I_d	vector influence functions for axial, radial and circumferential vortex elements respectively
I_A, ...	integrals of chordwise vortex distribution and decoupled kernel
$\mathcal{I}$	imaginary part of complex function
J	propeller advance ratio, $U/\Omega R_p$
K_m	kernel of final governing equations
N	blade number
P	"forcing function" of higher propeller harmonics
$Q_{n-\frac{1}{2}}(\tilde{\omega})$	Legendre function of second kind and half order
R	radius of the shroud camber surface in the propeller plane used as reference length
$\mathcal{R}$	real part of complex function
R_p	propeller semi-diameter
S_n	$(Q_{n+1/2}+Q_{n-3/2})$
T_n	$(Q_{n+1/2}-Q_{n-3/2})$
U	uniform free stream

c	shroud chord
g_{mN}, h_{mN}	functions dependent on higher harmonics of shed vorticity
$\underline{i}, \underline{j}, \underline{k}$	unit vectors in the Cartesian system (x,y,z)
$\underline{i}, \underline{i}_r, \underline{i}_\theta$	unit vectors in the cylindrical system (x,r,θ)
i	$\sqrt{-1}$
j	dummy summation index
ℓ	blade index number
m	rank of Fourier harmonic
n	order of Legendre function
p	static pressure
$\underline{q}$	fluid velocity
t	time variable
x, r, θ	cylindrical coordinates fixed in propeller
x_s, r_s, θ_s	cylindrical coordinates of point on shroud surface
x, y, z	Cartesian coordinates fixed in the propeller
x_s, y_s, z_s	Cartesian coordinates of point on shroud surface
$\bar{x}, \ldots$	nondimensional coordinates with respect to R ; e.g., $\bar{x} = x/R$
$\hat{x}, \ldots$	nondimensional coordinates with respect to R_p ; e.g. $\hat{x} = x/R_p$
γ	bound vortex shroud distribution
δ_{ij}	Kronecker delta
ϵ	shroud camber
ϵ_e	effective shroud camber

λ	shroud chord to diameter ratio, $c/2R$
μ	propeller tip to shroud radius ratio, R_p/R
ρ	constant fluid density
σ	$mU/\rho\mu$
τ	dummy time variable
$\bar{\tau}$	$\Omega\tau$
$\hat{\tau}$	$U\tau/R$
$\tilde{\omega}$	argument of Legendre function
$(\ )'$	denotes total differentiation of a function with respect to its argument
$\Gamma(r)$	bound blade circulation
$\bar{\Gamma}$	$\Gamma/R_p U$
Γ_M	maximum of $\bar{\Gamma}$
Γ_j	nondimensional Fourier coefficients of blade circulation
$\tilde{\Gamma}_M$	actuator disk limit of total maximum circulation
Δ	difference between element and field variable; e.g., $\Delta x = (x-x_v)$
θ	dummy angular variable of integration
χ_j	characteristic functions giving effective shroud camber
Ω	constant angular velocity of propeller

THREE-DIMENSIONAL THEORY OF DUCTED PROPELLERS

INTRODUCTION

Since the conception of the ducted propeller or Kort nozzle in the early 1930's[1,2], considerable interest has been aroused in this configuration, particularly for VTOL applications in recent years. Despite its promise, however, its inherent "parametric" complexity has precluded the achievement of comprehensive theoretical and experimental developments. Consequently, the design of an optimum ducted propeller has been impossible.

Previous theories have been reviewed by A. Sacks and J. Burnell[3], L. Meyerhoff and A. Finkelstein[4], and J. Megrue[5]. There are four main categories: (i) momentum methods, (ii) singularity distribution methods, (iii) "boundary value" or streamline methods, and (iv) combinations of, or approximations to, these methods. In general, though, the basic effects associated with a propeller of finite blade number are removed by its representation as a disk supporting a uniform pressure jump[6,7,8].

The objective of the present investigation is to derive a three-dimensional theory without the disk approximation. The simplest ducted propeller situation is chosen which retains most of the principal parameters and yet remains amenable to mathematical solution.

This case corresponds to the ducted propeller with discrete blading at zero angle of attack in a uniform, unbounded stream of inviscid, incompressible fluid. The shroud, blade and hub thicknesses are assumed to be zero and the shroud camber as well as the ratio of the blade chord to the shroud chord are considered small.

The appropriate theoretical model consists of a cylindrical surface of distributed vortices positioned with its axis coincident to a uniformly translating and rotating stream. The blades are introduced as individual, radial vortex lines of varying circulation with accompanying helical vortex sheets. The blade circulation distribution is specified arbitrarily.

Formulation of the problem follows the general procedure of thin lifting surface theory. The inherent periodicity of the shroud loading and the harmonic nature of the propeller field reduces the governing equations to decoupled, single integral form. Either directly or by modifications, solutions are expressible in terms of the results of J. Weissinger[9]. Certain self-sustaining shroud load distributions appear which seem analogous to the recent instability results of H. Ludwieg[10].

It is hoped that this solution will provide not only absolute information for design, optimization and experimental test programming, but may justify extended effort for the more difficult cases of angle-of-attack and static thrust.

CHAPTER ONE

BASIC FORMULATION

1.1 Physical Problem and General Background

The problem which we have chosen to study is a ducted propeller in steady forward flight at zero incidence in an incompressible fluid otherwise at rest. The forward velocity will be assumed sufficiently large and the shroud camber and blade loading low enough that the theory of linearized perturbations may be used. For this investigation the Reynolds number will be taken large enough to confine viscous effects to the boundary layer. This will be reasonably valid except in the neighborhood of the propeller tip if it penetrates the shroud boundary layer.

With respect to the geometry of the ducted propeller configuration, any thickness effects due to the hub, propeller blade or shroud will be postponed to subsequent investigations. However, the effective camber which they produce can readily be incorporated within the framework of the present analysis.

Because of the viscous skin drag associated with long shrouds, shrouds of moderate chord to diameter ratio are of principal interest. Fortunately, this is consistent with the usual thin airfoil approximations of satisfying the boundary conditions on the chordline by a bound vortex distribution on the chordline. Küchemann and Weber have sug-

gested a value of two as an upper limit to this ratio for finite length effects in their work on annular airfoils[6].

On the other hand, the ratio of the shroud chord to the blade chord is expected to be fairly large. That is, for conventional propeller blades, the aspect ratio is quite large and the shroud should be approximately of the same diameter as the propeller. Therefore in order to gain as much thrust improvement as possible by preventing slipstream contraction, the shroud has to be lengthened. Since this increases the viscous shear drag, an optimum configuration can exist. Sufficient for the moment, it is reasonable to take the shroud length much greater than the blade chord as stated.

In ordinary thin airfoil theory, we have two classes of problems: (i) the direct one in which the pressure or velocity on the airfoil is given and the airfoil geometry is to be determined; and (ii) the inverse problem in which the airfoil geometry is given and the pressure or velocity on the airfoil is to be determined. For the case we are examining here, we have two bodies, the shroud and the propeller, and hence we have four possibilities of combining the above appropriately. In other words, we have either (i) the direct-direct; (ii) the direct-inverse; (iii) the inverse-direct; or (iv) the inverse-inverse, where the first word refers to the shroud and the second, the propeller. In consideration of engineering applications, comparison with

experimental measurements, configuration optimization and possible boundary layer studies, the inverse-direct problem has been selected. Nevertheless, throughout much of the analysis, it is immaterial as to which case is considered.

The shroud geometry will be assumed as well as the blade circulation. We are not directly concerned with the chordwise loading of the blade or the determination of its geometry since we can replace it with a radial vortex spike by virtue of our shroud-blade-chord ratio assumption. The problem, then, will be to obtain the shroud pressure distribution.

To formulate the problem, appropriate singular solutions of Euler's equations will be distributed to represent the shroud, blades and their shed vortices. In general the strengths of these distributions will be determined from the requirement that the component of the total velocity normal to the shroud surface be zero and that the Kutta-Joukowski condition be satisfied along the shroud trailing edge.

1.2 Coordinate System

In a space-fixed coordinate system, the flow is unsteady due to both the motion of the duct and the propeller. The duct has the uniform translation U and the propeller, the constant rotation Ω as well as the translation U, see Fig. 1.1. Because of this rotation, the motion is also unsteady in a uniformly translating system fixed in the duct. However, consider a uniformly translating and rotating system

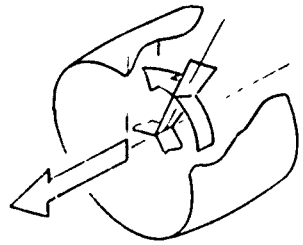

FIGURE 1.1

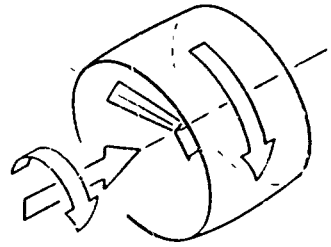

FIGURE 1.2

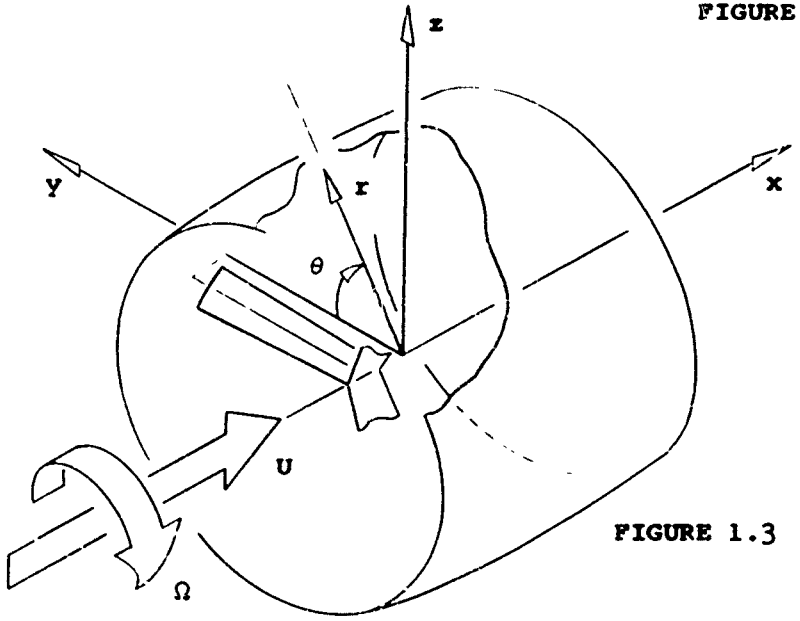

FIGURE 1.3

fixed to the propeller, say the Cartesian coordinates (x,y,z) or the equivalent cylindrical coordinates (x,r,θ). Increasing θ is chosen in accordance with the righthand rule for positive advance along the positive x-axis and is measured from the positive y-axis.

In this system, Fig. 1.2, we see that the incoming "free stream" has an axial component of magnitude U in the positive x-direction and a tangential component Ωr in the positive or increasing θ-direction. Now, the blades are at rest with respect to the propeller coordinates, but the duct is rotating with angular speed Ω about the propeller axis as shown. Since the duct is axisymmetrical about its axis of rotation and only the normal component of the velocity is required to vanish, the rotational motion of the duct does not affect the potential solution. In other words this motion is arbitrary and can be set equal to zero in the propeller-fixed coordinates. This mathematically equivalent model then corresponds to the physical case in which the shroud is rotating along with the propeller, see Fig. 1.3.

A simple case might illustrate this mathematical equivalence. Consider a two-dimensional thin airfoil in a uniform, inviscid stream. Then, suppose an infinitesimally thin belt is stretched around the airfoil and set into motion. For the resultant flow, the normal boundary and Kutta conditions are unaltered by this motion and so the solution is the same as before. In a real fluid, of course, the boundary

layer would be changed and hence also the potential flow, proportional to the modification of the effective airfoil shape. This correction is of higher order, however, and so, consistent with the usual thin airfoil approximations, the two are equivalent.

If the axis of the duct were inclined at an angle of attack α with respect to the translational motion, no equivalent steady flow would exist. That is, in this case there are time dependent incoming velocity components. With the stream U coincident with the xz-plane at time $t = 0$, we have for the free steam velocity $\underline{q}_U$ in propeller-fixed coordinates,

$$\underline{q}_U = U \cos \alpha \, \underline{i} + \Omega r \, \underline{i}_\theta + U \left[\sin (\theta - \Omega t) \, \underline{i}_r + \cos (\theta - \Omega t) \, \underline{i}_\theta \right] \sin \alpha \qquad (1.1)$$

Setting $\alpha = 0$, we see Eq. (1.1) reduces to the steady components U and Ωr we have already noted.

1.3 The Mathematical Model

With these considerations we can proceed to a detailed examination of the model. Fig. 1.4 gives the geometrical properties of the configuration. The plane

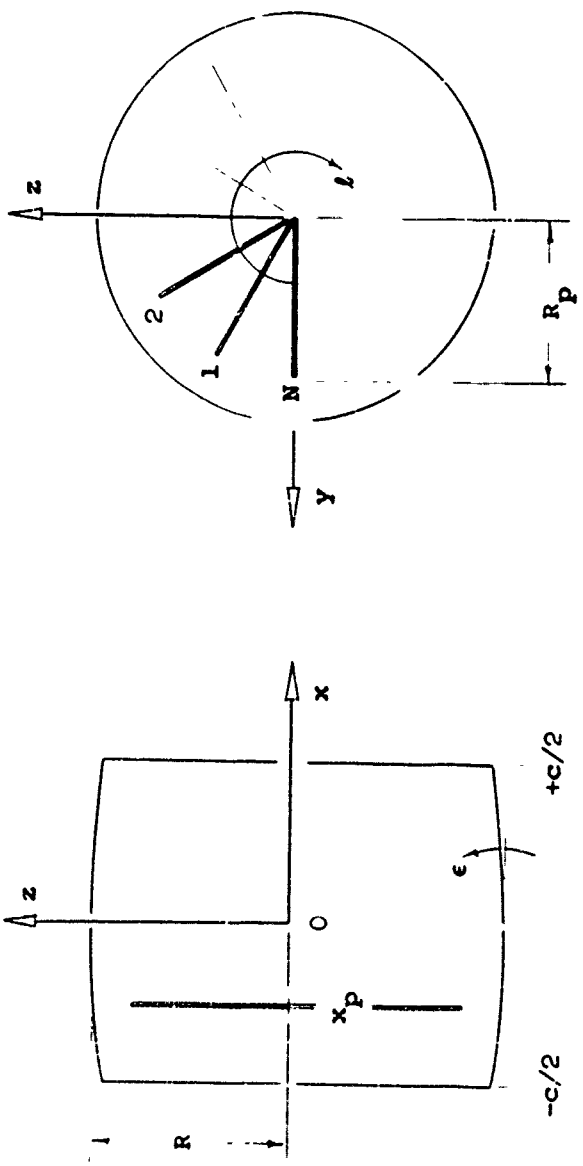

FIGURE 1.4

GEOMETRY OF DUCTED PROPELLER CONFIGURATION

determined by the leading edge of the duct is perpendicular to the x-axis at $x = -c/2$ and the trailing edge, at $x = +c/2$. The propeller disk of radius R_p is normal to the x-axis at $x = x_p$ with the N^{th} of the N blades lying in the xy-plane. The slope of the shroud with respect to the x-axis in any xr-plane is designated by $\tan \epsilon(x)$, which is taken positive for increasing shroud radius with increasing x . A reference shroud radius is R . For convenience with respect to tip clearance, R is taken as the radius of the shroud camber surface in the propeller plane.

In accordance with our assumptions, we can now represent the configuration by a distribution of bound and shed vortices. First, the propeller model follows classical theory. The circulation distribution of the bound radial vortex spikes replacing the blades is designated by $\Gamma(r_v)$, the subscript v being generally used to designate the location of a vortex element. Each blade, by symmetry, has identical loading and is accompanied by its shed semi-infinite helical vortex sheet of strength $d\Gamma/dr_v$ per unit radial length. The helical shape is assumed to be determined by the incoming stream components at r_v , its point of shedding. For the shroud we have a form of a lifting surface. The bound vortex distribution per unit length is $\gamma(x_v, \theta_v; r_s)$ where $r_s = r_s(x_s)$ denotes the radius of the shroud camber surface. Because of γ's angular dependence generated by the finite blade number, each vortex ring has a trailing vortex cylinder

made up of an infinite number of semi-infinite helical vortices of strength $(\partial\gamma/\partial\theta_v)(r_s d\theta)$. The positive senses of these vortices will be defined later.

For a given propeller loading, we can now formulate an equation to determine γ . Let $\underline{q}$ be the total velocity vector given by

$$\underline{q} = \underline{q}_U + \underline{q}_\Gamma + \underline{q}_{\Gamma'} + \underline{q}_\gamma + \underline{q}_{\gamma'} \tag{1.2}$$

where $\underline{q}_U$ has been defined previously and $\underline{q}_\Gamma$ is the velocity induced by the N bound blade vortices; $\underline{q}_{\Gamma'}$, by the shed blade vortex sheets; $\underline{q}_\gamma$, by the shroud bound vortices; and $\underline{q}_{\gamma'}$, by the shed shroud vortices. With $\underline{q} \cdot \underline{i}$ and $\underline{q} \cdot \underline{i}_r$ as the axial and radial components of $\underline{q}$ respectively, then for the flow to be everywhere tangent to the shroud, we require from Fig. 1.4,

$$\tan \epsilon(x_s) = \frac{\underline{q}(x_s, r_s, \theta_s) \cdot \underline{i}_r}{\underline{q}(x_s, r_s, \theta_s) \cdot \underline{i}} \tag{1.3}$$

where $r_s(x_s)$ has been defined. Eq. (1.3) is exact within our model limitations. If we assume $\epsilon \ll \pi/2$, $\tan \epsilon = \epsilon + O(\epsilon$ Thus for a moderately loaded propeller or $O(\Gamma/R_p U) \ll 1$, $\underline{q} \cdot \underline{i} = O(U)$ and hence from Eq. (1.3), $\underline{q} \cdot \underline{i}_r = O(\gamma) = O(U\epsilon)$ This leads to the linearization of the RHS of Eq. (1.3). Expanding $\underline{q} \cdot \underline{i}_r$ and $\underline{q} \cdot \underline{i}$ as

$$\underline{q}(x_s, r_s, \theta_s) \cdot \underline{i}_r = \underline{q}(x_s, R, \theta_s) \cdot \underline{i}_r + \left.\frac{\partial \underline{q} \cdot \underline{i}_r}{\partial r_s}\right|_{r_s=R} (r_s - R) + \ldots$$

$$\underline{q}(x_s, r_s, \theta_s) \cdot \underline{i} = \underline{q}(x_s, R, \theta_s) \cdot \underline{i} + \left.\frac{\partial \underline{q} \cdot \underline{i}}{\partial r_s}\right|_{r_s=R} (r_s - R) + \ldots \qquad (1.4)$$

and noting that $(r_s - R) = O(c\epsilon)$, we have to retain only the first terms from consideration of the previous orders. In addition, from Eq. (1.2) with $\alpha = C$ for $\underline{q}_{\gamma}$ of Eq. (1.1), the axial component can be replaced by U and Eq. (1.3) reduces to a familiar thin airfoil type approximation,

$$\epsilon(x_s) = \frac{\underline{q}(x_s, R, \theta_s) \cdot \underline{i}_r}{U} \qquad (1.5)$$

That is, we have only to satisfy a perturbation boundary condition on a mean shroud or reference surface. Since the radial component of the free stream is zero for zero angle of attack, Eq. (1.1), we have only to calculate the induced radial components. The bound and shed shroud vortices as formulated are located by r_s. But consistent with the orders we have retained, an expansion as carried out for $\underline{q} \cdot \underline{i}$ and $\underline{q} \cdot \underline{i}_r$ shows that use of the mean radius R is sufficient. In subsequent discussions, $\underline{q}_{\gamma}$ and $\underline{q}_{\gamma}$ will be so considered without further notation.

Eq. (1.5), together with a Kutta condition at the trailing edge of the shroud, is the basic equation for the determination of the shroud vorticity and hence the loading. The propeller inflow could also be calculated and hence the required blade geometry for the selected blade loading.

1.4 Velocity Influence Functions

In order to express the radially induced flow, or wash, of Eq. (1.5) as well as the inflow components, it is convenient to introduce three elementary velocity fields. These fields, or influence functions, $\underline{I}_h, \underline{I}_p, \underline{I}_d$ are due to vortices of unit strength and unit length which lie in the axial, radial and circumferential directions respectively as shown in Fig. 1.5

In general, then, we have from the Biot-Savart law for the velocity induced by an infinitesimal vortex in an incompressible fluid,

$$\underline{I}_h, \ \cdots = \frac{1}{4\pi} \frac{\underline{I} \times \underline{D}}{|\underline{D}|^3} \tag{1.6}$$

where $\underline{I}$ is a unit vector in the positive direction of our desired element and $\underline{D}$ is the vector from the element at (x_v, r_v, θ_v) to the field point (x, r, θ),

$$\underline{D} = (x-x_v)\,\underline{i} + (y-y_v)\,\underline{j} + (z-z_v)\,\underline{k} \tag{1.7}$$

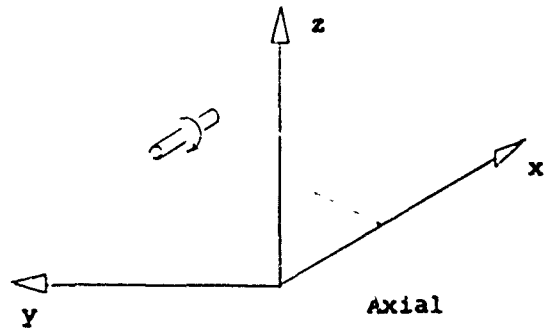

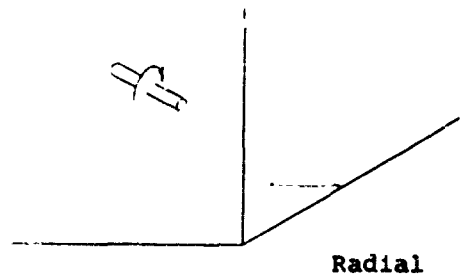

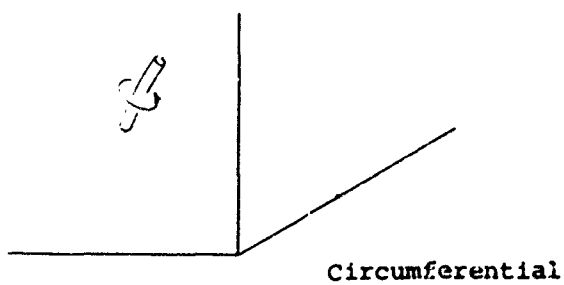

FIGURE 1.5

BASIC VORTEX ELEMENTS TO DESCRIBE THE FLOW FIELD

with the relation

$$x = x$$
$$y = r \cos \theta$$
$$z = r \sin \theta \tag{1.8}$$

between the cylindrical and Cartesian coordinate systems. The unit vectors $\underline{i}, \underline{j}$ and $\underline{k}$ are directed along the x,y and z-axes respectively.

From Fig. 1.5 we have for the axial element, or $\underline{I}_h$, simply

$$\underline{I} = \underline{i} \tag{1.9}$$

where positive circulation is chosen in accordance with a righthand screw advancing in the positive x-direction. For the radial element, or $\underline{I}_p$, again using the righthand rule, we have

$$\underline{I} = \cos \theta_v \, \underline{j} + \sin \theta_v \, \underline{k} \tag{1.10}$$

with positive circulation corresponding to advance in the positive radial direction. Finally, for the circumferential element, or $\underline{I}_d$,

$$\underline{I} = - \sin \theta_v \, \underline{j} + \cos \theta_v \, \underline{k} \tag{1.11}$$

for positive circulation in the increasing θ-direction. This sign convention on the shroud will turn out opposite to that usually employed in wing theory.

1.5 Calculation of the Induced Velocities

From $\underline{I}_p$ and $\underline{I}_d$, the velocity fields for both the propeller and shroud vortices may be simply expressed, and from $\underline{I}_h$ and $\underline{I}_d$, the fields of the shed helical vortices.

For $\underline{q}_\Gamma$, we integrate over each blade and sum the results over all blades. Or, from Fig. 1.4, we have

$$\underline{q}_\Gamma = \sum_{\ell=1}^{N} \int_0^{R_p} \Gamma(r_v)\, \underline{I}_p(x_p, r_v, 2\pi\ell/N)\, dr_v \tag{1.12}$$

where Eqs. (1.6) through (1.8) together with Eq. (1.10) give $\underline{I}_p$ and the argument of $\underline{I}_p$ locates a vortex element, the field point remaining unspecified for the moment. The index ℓ denotes the blade number, the N^{th} blade being chosen arbitrarily to coincide with the y-axis.

Likewise for the shroud, we have by integration over γ placed on the reference cylinder of radius R,

$$\underline{q}_\gamma = \int_{c/2}^{c/2} \int_{-\pi}^{\pi} \gamma(x_v, \theta_v)\, \underline{I}_d(x_v, R, \theta_v) R\, d\theta_v dx_v \tag{1.13}$$

$\underline{I}_d$ is given by Eqs. (1.6) through (1.8) and Eq. (1.11).

To express $\underline{q}_{\Gamma'}$ and $\underline{q}_{\gamma'}$, we require the velocity induced by a semi-infinite helical vortex of unit strength, with its axis coincident with the x-axis. As assumed, the shape is determined by the free stream. That is, the coordinates of any point on the helix which originates at (x_v, r_v, θ_v) are given by $(x_v+U\tau, r_v, \theta_v+\Omega\tau)$. Here τ is the conventional variable representing the time for a vortex element, convected by the free stream to travel from the point of shedding to that point. Subsequently, then, we recognize that the helical filament can be represented by an infinite series of component elements parallel and concentric to the x-axis. Integrating over these component elements of length $Ud\tau$ and $r_v\Omega d\tau$ respectively, we obtain the desired velocity field. This can be compared with the results of other propeller investigations, see T. Moriya[11], for example.

From Helmholtz's theorem, the strength per unit length of the vortices shed from the propeller is $-\Gamma'$. The prime denotes differentiation with respect to the argument and the adopted sign convention introduces the minus sign. Carrying the integration and summation over the propeller, we have

$$\underline{q}_{\Gamma'} = \sum_{\ell=1}^{N} \int_0^{R_p} -\Gamma'(r_v) \int_0^{\infty} (\underline{I}_h U + \underline{I}_d \, r_v \Omega) \, d\tau dr_v$$

where

$$\underline{I}_h \equiv \underline{I}_h(x_p+U\tau, r_v, 2\pi\ell/N, \Omega\tau)$$

$$\underline{I}_d \equiv \underline{I}_d(x_v+U\tau, r_v, 2\pi\ell/N+\Omega\tau) \tag{1.14}$$

$\underline{I}_h$ is given by Eqs. (1.6)-(1.8) and Eq. (1.9), and $\underline{I}_d$ was given for $\underline{q}_\gamma$. The integration over the dummy time parameter τ is identified as the velocity field of the semi-infinite helix of unit strength.

Finally, we can derive $\underline{q}_\gamma$, for the shroud, where the strength per unit length of the shed vortices is $-\partial\gamma/\partial\theta_v$. Integrating over the reference surface of radius R as for $\underline{q}_\gamma$,

$$\underline{q}_\gamma' = \int_{-c/2}^{c/2}\int_{-\pi}^{\pi} -\frac{\partial\gamma}{\partial\theta_v}\int_0^\infty (\underline{I}_h U+\underline{I}_d R\Omega)\, d\tau\, d\theta_v\, dx_v$$

where,

$$\underline{I}_h \equiv \underline{I}_h(x_v+U\tau, R, \theta_v+\Omega\tau)$$

$$\underline{I}_d \equiv \underline{I}_d(x_v+U\tau, R, \theta_v+\Omega\tau) \tag{1.15}$$

and $\underline{I}_h$ and $\underline{I}_d$ were previously noted.

Superposition of the velocity fields expressed by Eqs. (1.12), (1.13), (1.14) and (1.15) determine, within the limits of our approximation, the total induced velocity at any field point.

1.6 Formulation of Basic Equation for γ

With the total induced velocity field we can complete the explicit formulation of Eq. (1.5) for the shroud vortex distribution γ . In particular, we need only the radial components of the velocity evaluated on the reference surface.

To determine these components, we first carry out the required scalar triple products $\underline{i}_r \cdot \underline{I} \times \underline{D}$. The radial unit vector $\underline{i}_r$ is given by Eq. (1.10) with θ_v replaced by θ ; $\underline{I}$, by Eqs. (1.9), (1.10) and (1.11); and $\underline{D}$, by Eqs. (1.7) and (1.8). With $x = x_s$, $r = R$ and $\theta = \theta_s$, we have

$$\underline{i}_r \cdot \underline{I}_h \times \underline{D} = - r_v \sin (\theta_s - \theta_v) \tag{1.16}$$

$$\underline{i}_r \cdot \underline{I}_p \times \underline{D} = - (x_s - x_v) \sin (\theta_s - \theta_v) \tag{1.17}$$

$$\underline{i}_r \cdot \underline{I}_d \times \underline{D} = (x_s - x_v) \cos (\theta_s - \theta_v) \tag{1.18}$$

The other quantity we need is the magnitude of the vector $\underline{D}$ from any element to the field point given by

$$D^2 = \Delta x_v^2 + R^2 + r_v^2 - 2Rr_v \cos \Delta\theta_v \tag{1.19}$$

for field points on the shroud where $\Delta x_v \equiv (x_s - x_v)$ and $\Delta\theta_v \equiv (\theta_s - \theta_v)$.

The radial shroud velocity components now follow from Eqs. (1.12), (1.13), (1.14) and (1.15). For the propeller

contributions, the bound vortices give,

$$\underline{q}_\Gamma \cdot \underline{i}_r = -\frac{\Delta x_p}{4\pi}\sum_{\ell=1}^{N} \sin \Delta\theta_\ell \int_0^{R_p} \Gamma(r_v)\, D^{-3}\, dr_v \qquad (1.20)$$

where $\Delta x_p \equiv (x_s - x_p)$, $\Delta\theta_\ell \equiv (\theta_s - 2\pi\ell/N)$ and D is given by Eq. (1.19) with x_v replaced by x_p and θ_v , by $2\pi\ell/N$. For the shed vortices,

$$\underline{q}_{\Gamma'} \cdot \underline{i}_r = \frac{1}{4\pi}\sum_{\ell=1}^{N} \int_0^{R_p} r_v \Gamma' \int_0^{\infty} \{U \sin \Delta\theta_{\ell\tau} - \Omega\Delta x_{p\tau} \cos \Delta\theta_{\ell\tau}\}\, D^{-3}\, d\tau dr_v \qquad (1.21)$$

with $\Delta x_{p\tau} \equiv (x_s - x_p - U\tau)$, $\Delta\theta_{\ell\tau} \equiv (\theta_s - 2\pi\ell/N - \Omega\tau)$; and x_v replaced by $(x_p + U\tau)$ and θ_v by $(2\pi\ell/N + \Omega\tau)$ in D . For the bound shroud vortices, we have

$$\underline{q}_\gamma \cdot \underline{i}_r = \frac{R}{4\pi}\int_{-c/2}^{c/2} \Delta x_v \int_{-\pi}^{\pi} \gamma\, D^{-3} \cos \Delta\theta_v\, d\theta_v dx_v \qquad (1.22)$$

with r_v replaced by R in Eq. (1.19); and

$$\underline{q}_{\gamma'} \cdot \underline{i}_r = \frac{R}{4\pi}\int_{-c/2}^{c/2} \int_{-\pi}^{\pi} \frac{\partial\gamma}{\partial\theta_v} \int_0^{\infty} \{U \sin \Delta\theta_{v\tau} - \Omega\Delta x_{v\tau} \cos \Delta\theta_{v\tau}\}\, D^{-3}\, d\tau\, d\theta_v dx_v \qquad (1.23)$$

for the shed shroud vortices with $\Delta x_{v\tau} \equiv (x_s - x_v - U\tau)$, $\Delta\theta_{v\tau} \equiv (\theta_s - \theta_v - \Omega\tau)$; and x_v replaced by $(x_v + U\tau)$, r_v by R and θ_v by $(\theta_v + \Omega\tau)$ in Eq. (1.19).

If Eqs. (1.20), (1.21), (1.22) and (1.23) together with Eq. (1.19) are substituted into Eqs. (1.2) and (1.5), the basic equation for the shroud vorticity is determined in terms of a surface or double integral relation. As such it has the general form familiar to lifting surface theory. That is, for a specified propeller loading, the propeller terms may be grouped with the shroud camber term forming an effective camber. The shroud bound and shed vortices are then required to produce a flow tangent everywhere to this fictitious surface, as well as to satisfy a Kutta-Joukowski condition at the trailing edge.

Not only does this equation have this general form, but it may be compared in detail with the ring wing surface theory of J. Weissinger[9,12]. In fact if Ω is set equal to zero and the τ integration carried out, the form is identical with that of a modified ring wing having non-axisymmetric camber.

On the other hand, if the blade loading is not given, then a second equation must be written. In view of our approximation, a "lifting" line model would be appropriate. This equation would be coupled with Eq. (1.5) by the change in the effective local angle of attack of each blade element produced by the total inflow.

CHAPTER TWO

DERIVATION OF GOVERNING EQUATIONS

2.1 Periodic Expansion of Shroud Vortex Distribution

In general the inversion of a lifting surface type equation is exceedingly complex. However, in the present case as well as for a ring wing, the closing of the shroud surface introduces a natural periodicity which yields an essential simplification.

In particular the strength of the bound shroud vortices may be expanded in a complex Fourier series to permit integration over the θ_v variable, or

$$\gamma(x,\theta) \equiv U \sum_{m=-\infty}^{\infty} C_m(x)\, e^{imN\theta} \tag{2.1}$$

The speed U is inserted for convenience to non-dimensionalize certain subsequent expressions. Only mN components are used as indicated by the periodicity in $2\pi/N$ of the propeller velocities of Eq. (1.20) and (1.21) for the equal blade loading of the present case. Since γ is real, we require that the complex coefficients for positive (+m) and negative (-m) integers be complex conjugates, or

$$\begin{aligned} 2C_{-m} &= B_m + i\, A_m \\ 2C_{+m} &= B_m - i\, A_m \end{aligned} \tag{2.2}$$

where A_m and B_m are the real coefficients of the sine and cosine terms respectively of a trigonometric Fourier series over positive m for γ .

For $m = 0$, we note $A_0 = 0$ and $2C_0 = B_0$; i.e., $UB_0/2$ is the zeroth Fourier component of the shroud vorticity in the propeller-fixed coordinates, or equivalently, the time-independent part in the shroud-fixed coordinates. As such its physical role will be shown to determine the time average difference in shroud inner and outer static pressures.

2.2 Reduction of Shroud Contributions

Before substitution of Eq. (2.1) into Eqs. (1.22) and (1.23) for the shroud contributions to the radial velocities, we introduce the radius R as a reference length, or

$$\bar{x} \equiv x/R \ , \ \ldots \tag{2.3}$$

This will limit the explicit occurrence of the shroud chord to diameter ratio defined as

$$\lambda \equiv \frac{c}{2R} \tag{2.4}$$

to the limits of integration over the coefficients A_m and B_m . We also change our variable of integration from θ_v to $\Delta\theta_v/2$. Since the integrand is periodic in θ_v , we adjust the new limits of integration from $-\pi/2$ to $\pi/2$. In addi-

tion, the separation distance D is simplified by means of the cosine double angle formula.

Now using Eq. (2.1) in terms of the new quantities in Eq. (1.22), the order of integrations and summation may be interchanged because C_m has at worst a square root singularity at the shroud leading edge. We can then split out the θ_s dependence from the integrations to obtain,

$$\underline{q}_\gamma \cdot \underline{i}_r = U \sum_{m=-\infty}^{\infty} e^{imN\theta_s} \int_{-\lambda}^{+\lambda} C_m(\bar{x}_v)\, F_{\gamma m}(\Delta\bar{x}_v)\, d\bar{x}_v \qquad (2.5)$$

where,

$$F_{\gamma m} \equiv \frac{\Delta\bar{x}_v}{2\pi} \int_{-\pi/2}^{\pi/2} \frac{e^{-2imN\theta} \cos 2\theta}{(\Delta\bar{x}_v^2 + 4\sin^2\theta)^{3/2}}\, d\theta \qquad (2.6)$$

In other words, Eq. (2.5) represents the Fourier expansion of radial velocity induced on the shroud by the bound shroud vortices. The coefficients of this expansion are simply the integrals of the coefficients of the shroud vortices operated on by the functions of Eq. (2.6).

These functions may be simplified and expressed in terms of known functions. The sine term of the exponential is odd and $\cos 2\theta$ and $\sin^2\theta$, even, so that the imaginary part of $F_{\gamma m}$ is zero. For the real part we first note the trigonometric identity

$$2 \cos 2mN\theta \cdot \cos 2\theta = \cos 2(mN+1)\theta + \cos 2(mN-1)\theta \qquad (2.7)$$

and then use the trigonometric integral form of the Legendre function of the second kind and half order $Q_{n-\frac{1}{2}}$, developed under this program[13],

$$Q_{n-\frac{1}{2}}(\tilde{\omega}) = \int_{-\pi/2}^{\pi/2} \frac{\cos 2n\theta}{[2(\tilde{\omega}-1) + 4 \sin^2 \theta]^{\frac{1}{2}}} \, d\theta \qquad (2.8)$$

by differentiation with respect to the parameter $\tilde{\omega}$. Comparing the resulting forms, we have

$$F_{\gamma m} = - \frac{\Delta\bar{x}_v}{4\pi} S'_{mN}(\tilde{\omega}_1)$$

$$\tilde{\omega}_1 \equiv (1 + \Delta\bar{x}_v^2/2) \qquad (2.9)$$

where $S_{mN} \equiv (Q_{mN+1/2} + Q_{mN-3/2})$ and the prime denotes total differentiation.

Alternatively, $F_{\gamma m}$ may be expressed in complete elliptic integrals or Riegels' functions[13]. For the higher harmonics, the Legendre functions are more convenient. For any order they have the same logarithmic singularity at an argument of unity and decrease monotonically to zero for increasing argument, see Fig. 2.1. At any argument, they decrease monotonically with order. NBS tables[14], as well as extended tables[15] prepared under this study are available.

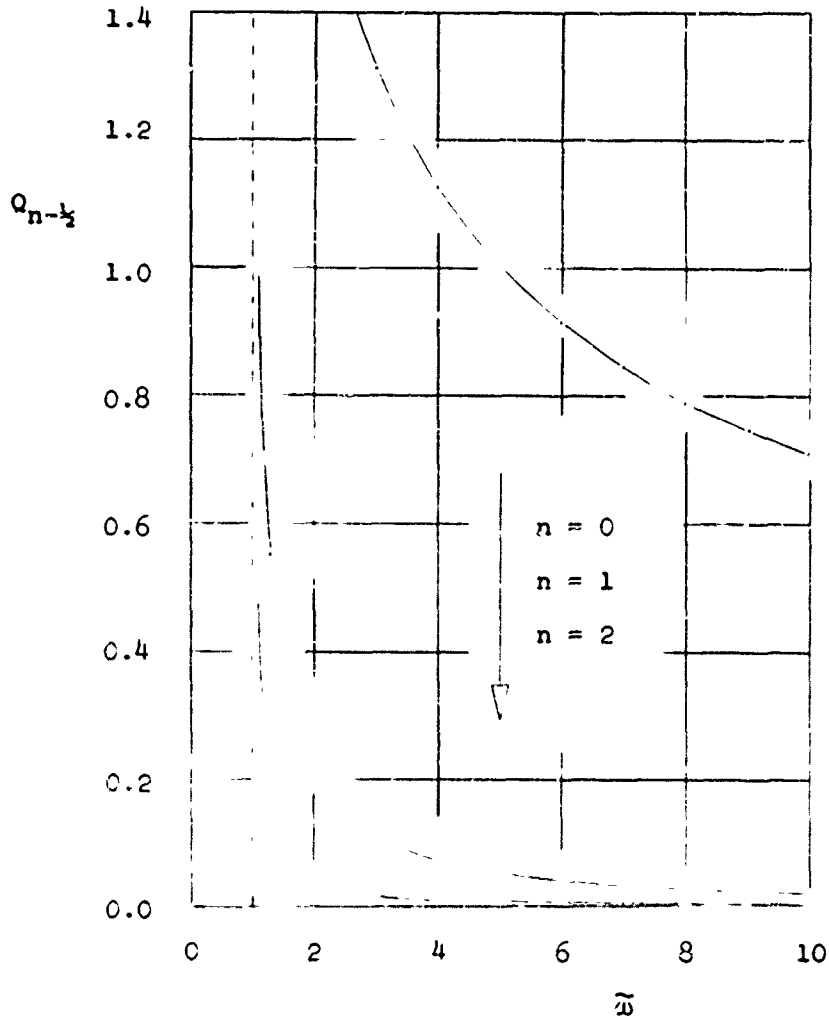

FIGURE 2.1

ILLUSTRATIVE BEHAVIOR OF THE LECENDRE FUNCTIONS OF THE SECOND KIND AND HALF ORDER

To derive an equation for the vortices shed from the shroud in a form like Eq. (2.5), we can proceed along similar lines. The only essential complication appears in the additional integration over the dummy time variable τ. Therefore, we interchange the order of integration of τ and θ_v and then use $\Delta\theta_{v\tau}/2$ as the variable of integration instead of θ_v. This gives a corresponding $F_{\gamma' m}$ in terms of an integration over the Legendre functions. That is, we find

$$\underline{q}_{\gamma'} \cdot \underline{i}_\tau = U \sum_{m=-\infty}^{\infty} e^{imN\theta_s} \int_{-\lambda}^{\lambda} C_m(\bar{x}_v)\, F_{\gamma' m}(\Delta\bar{x}_v)\, d\bar{x}_v \qquad (2.10)$$

where $F_{\gamma' m}$ is given by a Fourier integral over the dimensionless dummy time variable $\bar{\tau} \equiv \Omega\tau$, or

$$F_{\gamma' m} \equiv \frac{imN}{4\pi} \int_0^{\infty} e^{-imN\bar{\tau}} \left(\Delta\bar{x}_{v\tau} S'_{mN}(\tilde{\omega}_2) - iJ\mu\, T'_{mN}(\tilde{\omega}_2) \right) d\bar{\tau}$$

$$\tilde{\omega}_2 \equiv 1 + \Delta\bar{x}_{v\tau}^2/2 \qquad (2.11)$$

and $T_{mN} \equiv (Q_{mN+1/2} - Q_{mN-3/2})$. The product of the propeller advance ratio J and the propeller tip clearance parameter μ defined by

$$J \equiv U/\Omega R_p \tag{2.12}$$

$$\mu \equiv R_p/R \tag{2.13}$$

represent the "shroud advance ratio" $U/\Omega R$. The factor imN results from the differentiation of the shroud vorticity. This differentiation which is carried out termwise is justified on a physical basis.

2.3 Decomposition of Governing Equation for γ

The introduction of the expansion of Eq. (2.1) for γ has permitted the explicit integration over θ_v . If we now express the propeller contributions in terms of their Fourier components, we can decompose the single equation for the vortex distribution over the shroud surface into an infinite set of uncoupled equations integrated along the chord.

Let $UC_{\Gamma m}(\bar{x}_s)$ and $UC_{\Gamma' m}(\bar{x}_s)$ be the complex Fourier coefficients of the radial velocity induced on the shroud by the bound and shed propeller vortices, or

$$\underline{q}_\Gamma \cdot \underline{i}_r = U \sum_{m=-\infty}^{\infty} C_{\Gamma m} e^{imN\theta_s} \tag{2.14}$$

$$\underline{q}_{\Gamma'} \cdot \underline{i}_r = U \sum_{m=-\infty}^{\infty} C_{\Gamma' m} e^{imN\theta_s} \tag{2.15}$$

To find these coefficients we have, from orthogonality, the relations

$$C_{\Gamma m} = \frac{1}{2\pi U} \int_{-\pi}^{\pi} \underline{q}_{\Gamma} \cdot \underline{i}_{r} \, e^{-imN\theta_s} \, d\theta_s \tag{2.16}$$

$$C_{\Gamma' m} = \frac{1}{2\pi U} \int_{-\pi}^{\pi} \underline{q}_{\Gamma'} \cdot \underline{i}_{r} \, e^{-imN\theta_s} \, d\theta_s \tag{2.17}$$

for a period of 2π . Since $\underline{q}_{\Gamma} \cdot \underline{i}_{r}$ and $\underline{q}_{\Gamma'} \cdot \underline{i}_{r}$ are real quantities, the values of these coefficients corresponding to $+m$ and $-m$, must be complex conjugates.

First, substituting Eq. (1.20) into Eq. (2.16), we transform to the non-dimensional quantities previously used and interchange the order of the $\bar{r}_v$ - and θ_s - integrations. Since the θ_s dependence is periodic over the range of integration, we adjust the limits to $(-\pi + 2\pi\ell/N) \leq \theta_s \leq (\pi + 2\pi\ell/N)$ and integrate on $\theta \equiv \Delta\theta_\ell/2$ for $-\pi/2 \leq \theta \leq \pi/2$. The dependence over the blade summation index ℓ , then, disappears from this integral since it occurs only in the exponential power, $-2\pi m\ell_1$, which is equal to one for any integer $m\ell$. That is, for N identical blades, each blade contributes equally to any harmonic. The integral on θ itself, after removing a factor of $\bar{r}_v^{3/2}$ from $\bar{v}^3$, is evaluated in terms of the Legendre functions $Q_{n-\frac{1}{2}}$ by means of an equation analogous to Eq. (2.7) for the sine function, as well as Eq. (2.8).

The final result is,

$$C_{\Gamma m} = \frac{i\mu N \Delta\bar{x}_p}{8\pi^2} \int_0^{\mu} \frac{\bar{\Gamma}}{\bar{r}_v^{3/2}} T'_{mN}(\tilde{\omega}_3) d\bar{r}_v$$

$$\tilde{\omega}_3 \equiv 1 + [\ \Delta\bar{x}_p^2 + (1-\bar{r}_v)^2\ ]/2\bar{r}_v \qquad (2.18)$$

The non-dimensional blade circulation $\bar{\Gamma}$ is defined by,

$$\bar{\Gamma} \equiv \Gamma/R_p U \qquad (2.19)$$

Instead of U, ΩR_p could be used, but the translational speed is better for primary emphasis on the shroud.

If we substitute Eq. (1.21) into Eq. (2.17), we can proceed in the same way. The complication of the integration over the dummy time variable τ can be handled by an integration interchange corresponding to the analysis for the vortices shed from the shroud. Carrying this out, we find that

$$C_{\Gamma' m} = \frac{\mu N}{8\pi^2} \int_0^{\mu} \frac{\bar{\Gamma}'(\bar{r}_v)}{\bar{r}_v^{\frac{1}{2}}} \int_0^{\infty} e^{-imN\bar{\tau}} \{\ \Delta\bar{x}_{p\tau}\, S'_{mN}(\tilde{\omega}_4) - i J\mu\, T'_{mN}(\tilde{\omega}_4)\ \}\, d\bar{\tau}\, d\bar{r}_v$$

$$\tilde{\omega}_4 \equiv 1 + [\ \Delta\bar{x}_{p\tau}^2 + (1-\bar{r}_v)^2\ ]/2\bar{r}_v \qquad (2.20)$$

which is a Fourier integral.

In a broader sense, Eqs. (2.18) and (2.20) represent the harmonics of the radial velocity of a free propeller in an unbounded uniform stream. That is, x_s , R are interpreted as the coordinates of an arbitrary field point. S. Tsakonas and J. Breslin have determined the harmonic components[16] of the pressure field for a free propeller using the same vortex representation. Their results are expressed in complete elliptic integrals instead of Legendre functions.

Now, we substitute Eqs. (2.5), (2.10), (2.14), (2.15), (2.18) and (2.20) into Eq. (1.5) and equate the coefficients of each harmonic. After transposing the propeller terms, we obtain

$$\delta_{0m}\,\epsilon(\bar{x}_s) - C_{\Gamma m}(\Delta\bar{x}_p) - C_{\Gamma' m}(\Delta\bar{x}_p) = \int_{-\lambda}^{\lambda} C_m(\bar{x}_v)\,\{\,F_{\gamma m}(\Delta\bar{x}_v) + F_{\gamma' m}(\Delta\bar{x}_v)\,\}\,d\bar{x}_v \qquad (2.21)$$

where δ_{0m} is the Kronecker delta and m extends over all negative and positive integers. The shroud camber appears only in the zeroth harmonic since it is axisymmetric by assumption. In other words, in inviscid flow:

The effect of axisymmetric shroud camber for a ducted propeller at zero angle of attack appears only in the steady shroud load for a fixed blade loading.

2.4 Splitting of Governing Complex Equation

In complex form, Eq. (2.21) constitutes a doubly infinite set of equations over all m for the coefficients $C_m(\bar{x}_v)$ which determine the shroud vorticity. Alternatively, we can separate the real and imaginary terms, producing an infinite set of coupled pairs of equations in A_m and B_m over $m = 1,2,3 \ldots$.

For simplification, we note from the recursion relationship for the Legendre functions ,

$$Q'_{n-\frac{1}{2}} = Q'_{-n-\frac{1}{2}} \tag{2.22}$$

that,

$$\begin{aligned} S_{mN} &= S_{-mN} \\ T_{mN} &= -T_{-mN} \end{aligned} \tag{2.23}$$

From Eqs. (2.9) and (2.11), then, we have that $F_{\gamma,+m}$ and $F_{\gamma,-m}$ are complex conjugates and $F_{\gamma',+m}$ and $F_{\gamma',-m}$ are complex conjugates. That is,

$$\begin{aligned} F_{\gamma,+m} &= \mathcal{R}(F_{\gamma m}) \\ F_{\gamma,-m} &= \mathcal{R}(F_{\gamma m}) \\ F_{\gamma',+m} &= \mathcal{R}(F_{\gamma'm}) + i\mathcal{I}(F_{\gamma'm}) \\ F_{\gamma',-m} &= \mathcal{R}(F_{\gamma'm}) - i\mathcal{I}(F_{\gamma'm}) \end{aligned} \tag{2.24}$$

In addition, the propeller Fourier coefficients for $+m$ and $-m$ are complex conjugates. In fact, if Eqs. (2.23) are used in Eqs. (2.18) and (2.20), the equations for $C_{\Gamma,+m}$ and $C_{\Gamma,-m}$ are the same as for $F_{\gamma,+m}$ and $F_{\gamma,-m}$ with the real part replaced by the imaginary part, and the equations for $C_{\Gamma',+m}$ and $C_{\Gamma',-m}$ are exactly the same.

With these results and Eqs. (2.2), we can add and subtract [illegible] (2.21) into a set of coupled equations for A_m and B_m,

$$2\,\delta_{0m}\,\epsilon - 2\mathcal{R}(C_{\Gamma',m}) = \int_{-\lambda}^{\lambda} \{\, B_m \mathcal{R}(F_{\gamma m} + F_{\gamma',m}) + A_m\, \mathcal{I}(F_{\gamma',m}) \,\}\, d\bar{x}_v \qquad (2.25)$$

and,

$$-2\mathcal{I}(C_{\Gamma m}) - 2\mathcal{I}(C_{\Gamma',m}) = \int_{-\lambda}^{\lambda} \{\, -A_m \mathcal{R}(F_{\gamma m} + F_{\gamma',m}) + B_m\, \mathcal{I}(F_{\gamma',m}) \,\}\, d\bar{x}_v \qquad (2.26)$$

where $m = 0,1,2 \ldots$. For $m = 0$, $A_0 \equiv 0$ as noted before and Eq. (2.25) determines B_0.

The intermediate form of Eqs. (2.25) and (2.26) may be further simplified. First, from the recursion relation[13],

$$2nQ_{n-\frac{1}{2}} = Q'_{n+\frac{1}{2}} - Q'_{n-3/2} \tag{2.27}$$

the sin $mN\bar{\tau}$ term of $\mathcal{R}(C_{\Gamma',m})$, corresponding to the elements convected by the axial flow, may be reduced to $Q_{mN-\frac{1}{2}}$. On the other hand, the term produced by the swirl depends on $\Delta\bar{x}_{p\tau}$, but this is a perfect differential in $\bar{\tau}$; i.e.,

$$\frac{d}{d\bar{\tau}} S_{mN}(\tilde{\omega}_4) = -\frac{J\mu}{\bar{r}_v} \Delta\bar{x}_{p\tau} S'_{mN}(\tilde{\omega}_4) \tag{2.28}$$

Integrating this contribution to $\mathcal{R}(C_{\Gamma',m})$ by parts and noting $Q_{n-\frac{1}{2}}$ goes to zero at infinity, we get a contribution independent of $\bar{\tau}$ from the lower limit and can add the remaining integral to the reduced axial terms.

The term $\mathcal{I}(C_{\Gamma',m})$ yields to analogous steps while $\mathcal{I}(C_{\Gamma m})$ requires only Eq. (2.27). If we set $\mathcal{R}(2C_{\Gamma',m}) \equiv B_{\Gamma',m}$, $\mathcal{I}(2C_{\Gamma m}) \equiv -A_{\Gamma m}$ and $\mathcal{I}(2C_{\Gamma',m}) \equiv -A_{\Gamma',m}$, we get

$$B_{\Gamma',m} = \frac{N}{4\pi^2 J} \int_0^{\mu} \bar{\Gamma}' \bar{r}_v^{\frac{1}{2}} \left[S_{mN}(\tilde{\omega}_3) - g_{mN}(\Delta\bar{x}_p, \bar{r}_v) \right] d\bar{r}_v \tag{2.29}$$

$$A_{\Gamma m} = -\frac{\mu mN^2 \Delta\bar{x}_p}{2\pi^2} \int_0^{\mu} \frac{\bar{\Gamma}}{\bar{r}_v^{3/2}} Q_{mN-\frac{1}{2}}(\tilde{\omega}_3)\, d\bar{r}_v \tag{2.30}$$

$$A_{\Gamma',m} = \frac{N}{4\pi^2 J} \int_0^{\mu} \bar{\Gamma}' \bar{r}_v^{\frac{1}{2}} \left[h_{mN}(\Delta\bar{x}_p, \bar{r}_v) \right] d\bar{r}_v \tag{2.31}$$

The functions g_{mN} and h_{mN} are Fourier integrals given by:

$$g_{mN} \equiv mN \int_0^\infty \left[\frac{2(J\mu)^2}{\bar{r}_v} Q_{mN-\frac{1}{2}} + S_{mN} \right] \sin mN\bar{\tau}\, d\bar{\tau}$$

$$h_{mN} \equiv mN \int_0^\infty \left[\frac{2(J\mu)^2}{\bar{r}_v} Q_{mN-\frac{1}{2}} + S_{mN} \right] \cos mN\bar{\tau}\, d\bar{\tau} \qquad (2.32)$$

with $Q_{mN-\frac{1}{2}}$ and S_{mN} having the argument $\tilde{\omega}_4$.

Turning to the kernels of Eqs. (2.25) and (2.26), we find that they can be expressed in similar, but simpler, terms. In fact, we can show that one is proportional to the derivative of the other, or,

$$\mathcal{R}(F_{\gamma m} + F_{\gamma' m}) = - \frac{J\mu}{mN} \frac{d}{d\, \Delta\bar{x}_v} \mathcal{I}(F_{\gamma' m}) \qquad (2.33)$$

Therefore, we can define a single kernel, say $K_m \equiv (J\mu/mN) \cdot \mathcal{I}(F_{\gamma' m})$, and obtain

$$K_m(\Delta\bar{x}_v) = \frac{1}{4\pi} \left\{ S_{mN}(\tilde{\omega}_1) - g_{mN}(\Delta\bar{x}_v, 1) \right\} \qquad (2.34)$$

where the argument of $Q_{mN-\frac{1}{2}}$ and S_{mN} of $g_{mN}(\Delta\bar{x}_v, 1)$ is $\tilde{\omega}_2$ because $\bar{r}_v$ is unity. $-\Delta\bar{x}_v S'_{mN}(\tilde{\omega}_1)/4\pi$ is readily identified as $\mathcal{R}(F_{\gamma m})$ or the contribution of the bound vortices.

From Eqs. (2.29) through (2.34), the intermediate forms of Eqs. (2.25) and (2.26) assume the final forms,

$$2\delta_{0m}\,\epsilon - B_{\Gamma' m} = \frac{mN}{J\mu}\int_{-\lambda}^{\lambda} A_m K_m d\bar{x}_v - \int_{-\lambda}^{\lambda} B_m K'_m d\bar{x}_v \qquad (2.35)$$

$$A_{\Gamma m} + A_{\Gamma' m} = \frac{mN}{J\mu}\int_{-\lambda}^{\lambda} B_m K_m d\bar{x}_v + \int_{-\lambda}^{\lambda} A_m K'_m d\bar{x}_v \qquad (2.36)$$

where ϵ is a function of $\bar{x}_s$; $A_{\Gamma m}$, $A_{\Gamma' m}$, and $B_{\Gamma' m}$, of $(\bar{x}_s - \bar{x}_p)$; A_m and B_m , of $\bar{x}_v$; and K_m , of $(\bar{x}_s - \bar{x}_v)$. For $m = 0$, $A_0 \equiv 0$ and Eq. (2.35) determines B_0 .

2.5 Discussion of Coupled Equations

Eqs. (2.35) and (2.36) for the bound chordwise distributions of the shroud vorticity contain several important features

First, the propeller contributions depend only on the axial separation of the shroud point and the propeller plane for a given number of blades, blade loading and tip clearance. Since they do not depend on the angular position of the blade, the effect of finite blade chord could be incorporated in the present formulation. That is, the blade could be represented by a distribution of radial elements with $\theta_\ell = \theta_\ell(\bar{x}_p)$ and $\Gamma = \Gamma(\bar{r}_v, \bar{x}_p)$. The corresponding propeller Fourier coefficients would then be integrated over the appropriate range of $\bar{x}_p$.

Second, the coupling of the equations is due to the swirl, or Ω, of the incoming flow. In other words, from the intermediate forms of Eqs. (2.25) and (2.26), the equations would be independent only if $\partial(F_{\gamma,m})$ were zero. But from Eq. (2.11 this requires that $\Omega \to 0$. To see this, we resubstitute $\bar{\tau} = \Omega\tau$ and use the alternative dimensionless time $\hat{\tau} \equiv U\tau/R$. Then the exponential factor becomes one as $\Omega \to 0$ and the swirl terms disappear, giving the real quantity

$$\lim_{\Omega \to 0} F_{\gamma,m} = \frac{mN}{4\pi} \int_0^\infty T'_{mN}(\tilde{\omega}_2)\, d\hat{\tau} \tag{2.37}$$

where $\tilde{\omega}_2 = 1 + (\Delta\bar{x}_v - \hat{\tau})^2/2$. The decoupled equations have the same kernel K'_m which has a Cauchy singularity.

Third, various singularities will appear in our governing equations. In general the propeller contributions will remain finite since $\mu < 1$. For the limiting case of $\mu \to 1$, a special study of the anticipated behavior of the bound blade circulation near the tip is necessary. On the other hand, the chordwise distributions of the bound shroud vortices and the kernels will possess infinities. The coefficients A_m and B_m will have square-root singularities at the leading edge of the shroud since the fluid must usually flow around an edge of zero radius. Under special conditions of tangential flow entry at the leading edge, these singularities will disappear. The kernels will always be singular at the zero of their argu-

ment, however. That is, in integrating over the shroud we must always pass over a contributing element. To determine the nature of these singularities, we need the logarithmic behavior of the Legendre functions near unity. From Ref. 13, we have

$$Q_{n-\frac{1}{2}}(\tilde{\omega}) = \tfrac{1}{2}\ell n(\tilde{\omega}-1) + O(\tilde{\omega}-1)\ \ell n(\tilde{\omega}-1) \tag{2.38}$$

The integrand of $g_{mN}(0,1)$, then, has a $\bar{\tau}\ \ell n\ \bar{\tau}$ behavior near the lower limit, the only region of concern. Since this is bounded, $g_{mN}(\Delta\bar{x}_v,1)$ is regular at $\Delta\bar{x}_v = 0$. But, S_{mN}, the remaining term in K_m, gives two equal logarithmic contributions and Eq. (2.34) becomes,

$$K_m(\Delta\bar{x}_v) \sim -\frac{1}{2\pi}\ \ell n|\Delta\bar{x}_v| \tag{2.39}$$

near $\Delta\bar{x}_v = 0$ and the integral of Eqs. (2.35) and (2.36) must be interpreted in the Cauchy principal value sense. This singularity is due to the shed vortices which, in the neighborhood of $\Delta\bar{x}_v = 0$, appear as a semi-infinite sheet of vortices of constant strength. In contrast, differentiating Eq. (2.39), we have the usual Cauchy singularity of two-dimensional airfoil theory. Because $-\Delta\bar{x}_v S'_{mN}(\tilde{\omega}_1)/4\pi$ is the bound shroud vorticity contribution, this result is anticipated. In fact with neither swirl nor propeller terms, Eqs. (2.35) and (2.36) reduce to the zeroth harmonic for B,

which represents an axisymmetric ring at zero angle of attack in a uniform stream U. For the limiting case of infinite duct radius, the regular part of the kernel vanishes, leaving the singular part as the proper result.

Fourth, after removing the swirl, the decoupled equations are identified with the general equations for an infinitely thin ring wing as developed by Weissinger[9]. For the propeller and camber terms, this simply requires their reinterpretation as the coefficients of a trigonometric expansion for any specified radial wash that the shroud system must cancel. For the kernel, though, we need to show that the sum of the contributions from Eqs. (2.9) and (2.37) equals his results. The Cauchy singularity, as we have seen, coincides with the singularity of his kernel. This comes from the "bound" term $-\Delta\bar{x}_v s'_{mN}/4\pi$, which is invariant with the swirl and which is equated to its counterpart simply by the relation[13] between $Q_{n-\frac{1}{2}}$ and the Riegels function[17] G_n,

$$Q_{n-\frac{1}{2}}(\tilde{\omega}_1) = -\kappa^3 G_n(\kappa^2)/4 \tag{2.40}$$

where $\kappa^2 \equiv 2/(\tilde{\omega}_1+1)$. To equate $-g'_{mN}(\Delta\bar{x}_v,1)/4\pi$ and its counterpart, or the "shed" terms, is more difficult. One way is to re-express T'_{mN} in the Legendre integral form of Eq. (2.8) and interchange the order of integration. Integration on τ represents a semi-infinite straight vortex and can be carried out. The remaining integration then agrees with the corresponding Weissinger terms in integral form. Since, in

turn, he expresses these in Riegels functions, the final identity by means of Eq. (2.40) becomes for $mN \neq 0$,

$$\int_0^\infty T'_{mN}(\tilde{\omega}_2)\, d\hat{\tau} = \pi + \Delta\bar{x}_v\, T'_{mN} - \pi\, \Delta\bar{x}_v^3 \left(Q'_{mN-\frac{1}{2}} + 2Q'_{mN-3/2} \cdots + 2Q'_{\frac{1}{2}} + Q'_{-\frac{1}{2}} \right) \qquad (2.41)$$

a result which is needed later. The arguments on the RHS are $\tilde{\omega}_1$.

2.6 Shroud and Propeller Loading

After the determination of the shroud vortex distributions, the total perturbation velocities induced by the ducted propeller system may be computed at an arbitrary field point. This permits the calculation of the shroud pressure loadings as well as the propeller inflow velocities.

The required velocities $\underline{q}_\Gamma$, $\underline{q}_{\Gamma'}$, $\underline{q}_\gamma$ and $\underline{q}_{\gamma'}$ are given in general by Eqs. (1.12), (1.13), (1.14) and (1.15). Any component of the flow is evaluated by taking the appropriate scalar dot product into a unit vector in the desired component direction. Reduction to harmonic expressions in terms of the tabulated Legendre functions of second kind and half order follows the previous derivations.

To find the pressure, we use a linearized form of Bernoulli's equation. In the propeller-fixed coordinates, the flow is steady but rotational. Therefore the total head,

or static plus dynamic pressure, is constant only along a streamline ψ . That is,

$$p + \rho \underline{q} \cdot \underline{q}/2|_{\psi} =$$

$$p_{\infty} + \rho(U^2 + \Omega^2 r^2)/2 \qquad (2.42)$$

where p is the static pressure and ρ is the fluid density. By our assumption of small disturbances, the deflection of any streamline is negligible in Eq. (2.42), and we may use the same radius r for p and $\underline{q}$ as at infinity. Omitting the higher order velocity terms as before, we have for $\Delta p \equiv (p-p_{\infty})$,

$$\Delta p = - \rho \underline{q}_U \cdot \{ \underline{q}_\Gamma + \underline{q}_{\Gamma'} + \underline{q}_\gamma + \underline{q}_{\gamma'} \} \qquad (2.43)$$

with $\underline{q}_U$ from Eq. (1.1) for $\alpha = 0$. Only the axial and tangential components of $\underline{q}_\Gamma$, ... are necessary because $\underline{q}_U$ does not have a radial component.

From Eq. (2.43) and the induced velocities, the inner and outer shroud pressure distributions may be computed. In detail, these calculations are quite complex, but the net loading, or the inner pressure minus the outer pressure $\Delta p]$ is simply,

$$\Delta p] = -\rho U \gamma \qquad (2.44)$$

This we find from the Kutta-Joukowski force on a bound vortex element or from Eq. (2.43) since the only discontinuous velocity component at the element is produced by the element itself and is in a plane normal to the element. The leading edge force, if present, may be calculated in the usual manner from the coefficient of the singular term of the Glauert series for A_m and B_m.

Calculation of the axial and tangential components of the induced velocities at the propeller plane will provide the inflow quantities corresponding to the given loading. With these quantities, the blade angle settings and forces can be computed from the usual propeller blade element theory[18] of S. Drzewiecki. Since the inflow is due to all the vortex elements, the result is analogous to the Prandtl lifting line approximation for wings of moderate aspect ratio and is consistent with our representation of the blade as a vortex spike.

CHAPTER THREE

SOLUTIONS FOR DUCT LOADING

3.1 Fundamental Solution

The zeroth harmonic of the shroud vorticity distribution in propeller-fixed coordinates is independent of angular position on the shroud for a given chordwise position. On the other hand, if we transform to duct-fixed coordinates, we see that this harmonic corresponds to the time-independent part of the shroud vortex distribution. As such, it gives the average or fundamental duct loading.

Setting m equal to zero in Eq. (2.35), then, we obtain,

$$2\epsilon(\bar{x}_\varepsilon) - B_{\Gamma'0}(\Delta\bar{x}_p) = -\int_{-\lambda}^{\lambda} B_0(\bar{x}_v)\, K_C'(\Delta\bar{x}_v)\, d\bar{x}_v \qquad (3.1)$$

where the kernel $-K_C'$,

$$-K_C' = -\frac{\Delta\bar{x}_v}{2\pi} Q_{\frac{1}{2}}'(1 + \Delta\bar{x}_v^2/2)$$

is simplified by the reduction of the "bound" terms from Eq. (2.22) and by the absence of the "shed" terms. In fact, Eqs. (1.22) and (2.8) show that $-K_C'/R$ is the radial velocity influence function of a ring vortex of constant unit strength evaluated at the same radius R.

From Eq. (2.39), the singular part of the kernel is $1/2\pi\Delta\bar{x}_v$. Removing this, we have plotted the regular part of

$-2\pi K_0'$, which is antisymmetric, in Fig. 3.1 and tabulated the values in Table 3.1 for $0 \leq \Delta\bar{x}_v \leq 1$. The regular part represents the three-dimensional effect of the vortex ring. From Eq. (2.38), it behaves as $\Delta\bar{x}_v \ln \Delta\bar{x}_v$ at the origin, increases to a maximum, and then decays monotonically. The computational procedures followed those developed for the Legendre functions[15], and the results agree with Weissinger's alternate calculation[9] , or $U_0(\eta)$, where η corresponds to $\Delta\bar{x}_v$.

The propeller contribution is also simplified for $\lambda = 0$. From Eqs. (2.22), (2.29) and (2.32), we find

$$B_{\Gamma' 0} = \frac{N}{2\pi^2 J} \int_0^{\mu} \bar{\Gamma}'(\bar{r}_v)\, Q_{\frac{1}{2}}(\tilde{\omega}_3)\, \bar{r}_v^{\frac{1}{2}}\, d\bar{r}_v \qquad (3.2)$$

A priori, we might not anticipate this non-periodic contribution, but its identity will be established later.

Since $B_{\Gamma' 0}$ appears in parallel with the camber term, we see that it is of considerable significance. Without the propeller term, Eq. (3.1) is the equation for a ring wing at zero angle of attack. Consequently, the fundamental solution for the ducted propeller may be taken from this ring wing solution by using an <u>effective camber</u> ϵ_e ,

$$\epsilon_e \equiv \epsilon - B_{\Gamma' 0}/2 \qquad (3.3)$$

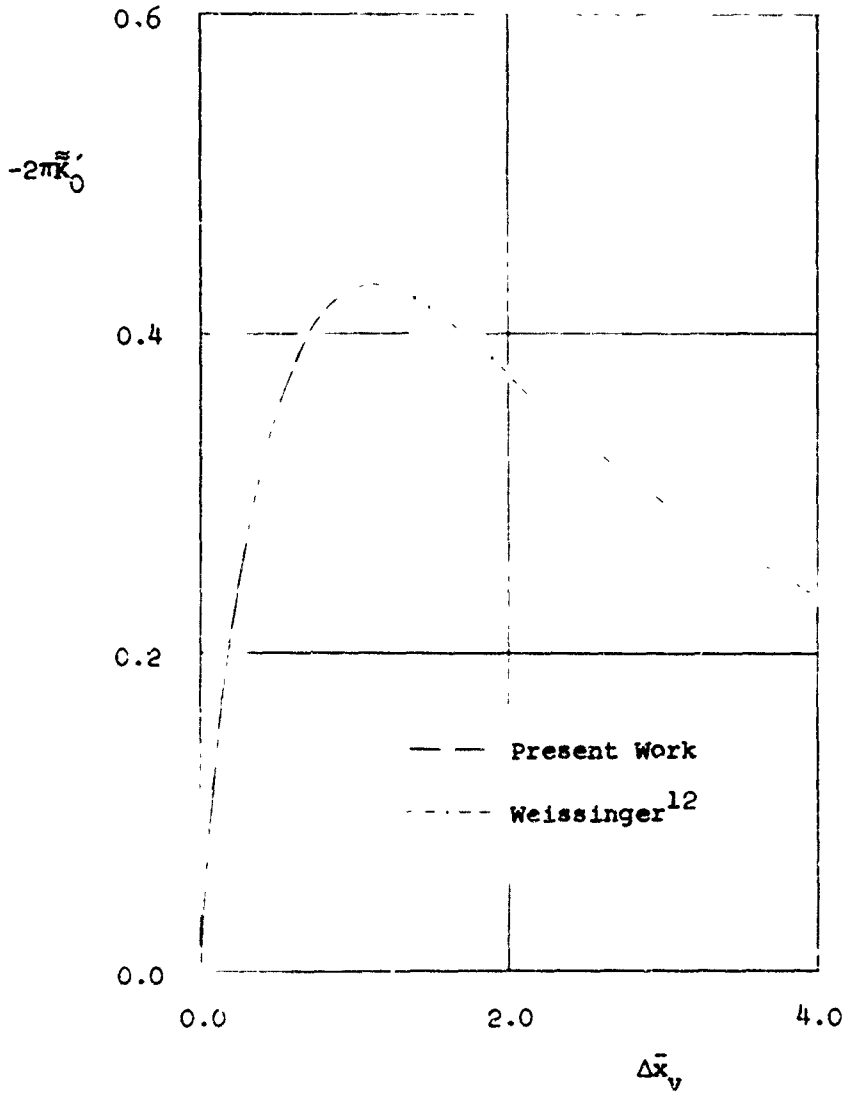

FIGURE 3.1

BEHAVIOR OF REGULAR PART OF KERNEL FOR ZEROTH HARMONIC

$$\tilde{\bar{K}}_0' = K_0' + 1/2 \quad \bar{x}_v$$

TABLE 3.1

REGULAR PART OF KERNEL FOR ZEROTH HARMONIC

$\Delta\bar{x}_v$	$-2\pi K_0' - 1/\Delta\bar{x}_v$
0.00	0.00000
0.05	0.07981
0.10	0.13290
0.15	0.17629
0.20	0.21305
0.25	0.24482
0.30	0.27253
0.35	0.29683
0.40	0.31815
0.45	0.33684
0.50	0.35322
0.55	0.36751
0.60	0.37989
0.65	0.39058
0.70	0.39966
0.75	0.40734
0.80	0.41370
0.85	0.41889
0.90	0.42298
0.95	0.42610
1.00	0.42833

In other words:

The mean pressure difference across the shroud of a ducted propeller at zero incidence in a uniform flow is identical to that of a similar ring wing of different camber.

Thus, experimental measurements on ring wings by O. Ladurner[19] and others, the rheoelectric analogy of L. Malavard[20], and the theoretical methods of Weissinger[9] can be applied to ducted propellers. Two points should be noted. First, this result is exactly valid only within the approximations of a linearized theory and of an inviscid fluid. Second, the shroud does not have to be of zero thickness. Though they do alter the effective camber, thickness effects can be superimposed[21,22] within the limitations of thin airfoil theory. In fact, with respect to the shroud thickness, they are identical for a ducted propeller and its equivalent ring wing.

3.2 Effect of Parameters on the Fundamental Load

The modification to the effective camber by the propeller for the fundamental solution depends on the following parameters

(i) Blade number

(ii) Blade circulation strength

(iii) Advance ratio

(iv) Tip clearance

(v) Propeller position

(vi) Strength of the vortices shed from the blades

To the extent, then, that camber effects are known for the ring wing, the effects of these parameters on ϵ_e determine their influence on the steady shroud load.

To study ϵ_e we express the blade circulation in a general form. In particular, in most cases for no loading at the root and finite tip clearance, the circulation distribution will be zero at $\bar{r}_v = 0$, without a hub, and at $\bar{r}_v = \mu$. Therefore, we take

$$\bar{\Gamma} = \Gamma_M \sum_{j=1}^{\infty} \Gamma_j \sin j\pi \hat{r}_v \tag{3.4}$$

where Γ_M, for convenience, is the maximum value of $\bar{\Gamma}$ and $\hat{r}_v \equiv \bar{r}_v/\mu$. From Fourier analysis, we have,

$$\Gamma_j = 2\int_0^1 \frac{\bar{\Gamma}}{\Gamma_M} \sin j\pi \hat{r}_v \, d\hat{r}_v \tag{3.5}$$

to determine the coefficients.

With the blade circulation distribution of Eq. (3.4) the propeller contribution $B_{\Gamma'0}$ to the effective camber becomes

$$B_{\Gamma'0} = \frac{N\Gamma_M\mu^{\frac{1}{2}}}{2\pi J} \sum_{j=1}^{\infty} j\Gamma_j \, X_j(\Delta\bar{x}_p, \mu) \tag{3.6}$$

after interchange of the order of summation and integration.

The characteristic functions χ_j are given by

$$\chi_j \equiv \int_0^1 \hat{r}_v^{\frac{1}{2}}\, Q_{\frac{1}{2}}(\tilde{\omega}_3) \cos j\pi\hat{r}_v \, d\hat{r}_v$$

$$\tilde{\omega}_3 = 1 + \frac{\Delta\tilde{x}_p^2 + (1-\mu\hat{r}_v)^2}{2\mu\hat{r}_v} \tag{3.7}$$

In the form of Eq. (3.6), the dependence of $B_{\Gamma'0}$ on the various parameters can be examined.

The simplest dependence is on the blade number, magnitude of the blade loading and the advance ratio. For the first two, the propeller camber contribution varies linearly in a uniform fashion along the duct. When N or Γ_M is zero, $B_{\Gamma'0}$ is zero as required. On the other hand, it is inversely proportional to the advance ratio. As $J \to 0$ either by $U \to 0$ or $\Omega \to \infty$, $B_{\Gamma'0}$ becomes infinite, which corresponds to the collapse of the shed propeller vortices into a disk of concentric vortices of infinite strength at the propeller plane. In contrast, when the advance ratio becomes infinite, the camber modification disappears. We may interpret this result in the following way. $B_{\Gamma'0}$ depends only on the variation of the blade circulation and not on the blade circulation itself. That is, the only reason we have an effect at all for finite advance ratios is the essential "smearing" of the basic periodic character of the blades by their shed vortices as they rotate out of the radial-axial planes in which they were shed. For infinite advance ratio, the shed

vortices trail back axially. Then there is no smearing and consequently no effective camber.

The influence of the three remaining parameters, the blade circulation profile or Γ_j's , the propeller position $\bar{x}_p$, and the tip clearance variable μ is not so easily obtained. Analytically, we see from Eq. (3.7) that each characteristic function is symmetric about the propeller plane. Since the corresponding integration of χ_j from 0 to $\bar{x}_s$ is antisymmetric, the equivalent shroud shape "induced" by the j^{th} Fourier component of the blade loading is antisymmetric with an inflection point at $\Delta\bar{x}_p = 0$. Differentiation of χ_j with respect to $\Delta\bar{x}_p$ shows that the slope of this induced camberline or contribution to the effective camber is a finite maximum or minimum at the propeller plane; i.e., $\partial\tilde{\omega}_3/\partial\Delta\bar{x}_p = \Delta\bar{x}_p/\mu\hat{r}_v \to 0$. The result is valid for the complete range of $0 \leq \mu \leq 1$ as verified by the logarithmic behavior of the Legendre function near its singularity and its asymptotic behavior[13] of $\bar{r}_v^{3/2}$ as $\bar{r}_v \to 0$. This agrees with the usual streamline patterns depicted for a propeller which show larger radial velocities nearer the propeller.

To furnish further insight as well as practical working figures, we have computed the characteristic functions for $j = 1,2,3,4,5$ at values of $\mu = 0.75$, 0.90 , 0.95 and 0.99 If the propeller plane is kept within the shroud, the maximum range of $\Delta\bar{x}_p$ required for any calculation is 2λ . We have

considered values of $0 \leq \Delta\bar{x}_p \leq 1$ or a minimum of $\lambda = 0.5$ for the case of the propeller plane at the shroud entrance or exit. For a centrally located propeller, the maximum of $\lambda = 1$ is attained.

The results are given in Figs. 3.2, 3.3, 3.4, and 3.5 along with their tabulated values in Tables 3.2, 3.3, 3.4 and 3.5. As previously noted, the greatest effects occur at the propeller plane and decay with increasing axial separation. The decay is faster for the higher harmonics. Analogous behavior is found for μ or radial separation and is illustrated in Fig. 3.6, a cross plot of the absolute values of χ_j at $\Delta\bar{x}_p = 0$. The tabulation is accurate to 10^{-4} or better.

As the tip clearance decreases we know, for a constant geometry, that the load near the tip does not generally decay so early and that the subsequent shed vortex grows in strength[23]. In the ideal flow, however, this vortex disappears when the tip just touches the shroud and $\Gamma' = 0$. The effect of the tip vortex, then, may be examined by assuming a constant blade circulation throughout the blade and approximating the tip behavior by a step function. Substituting $\bar{\Gamma} = \Gamma_M \, 1(\mu - \bar{r}_v)$ into Eq. (3.2) and evaluating the integral, we get

$$B_{\Gamma 0} = \frac{N\Gamma_M \mu^{\frac{1}{2}}}{2\pi^2 J} \, Q_{\frac{1}{2}} \left[1 + \frac{\Delta\bar{x}_p^2 + (1-\mu)^2}{2\mu} \right] \tag{3.8}$$

Consequently, the contribution of a tip vortex of strength Γ_M to the effective shroud camber can be found from the

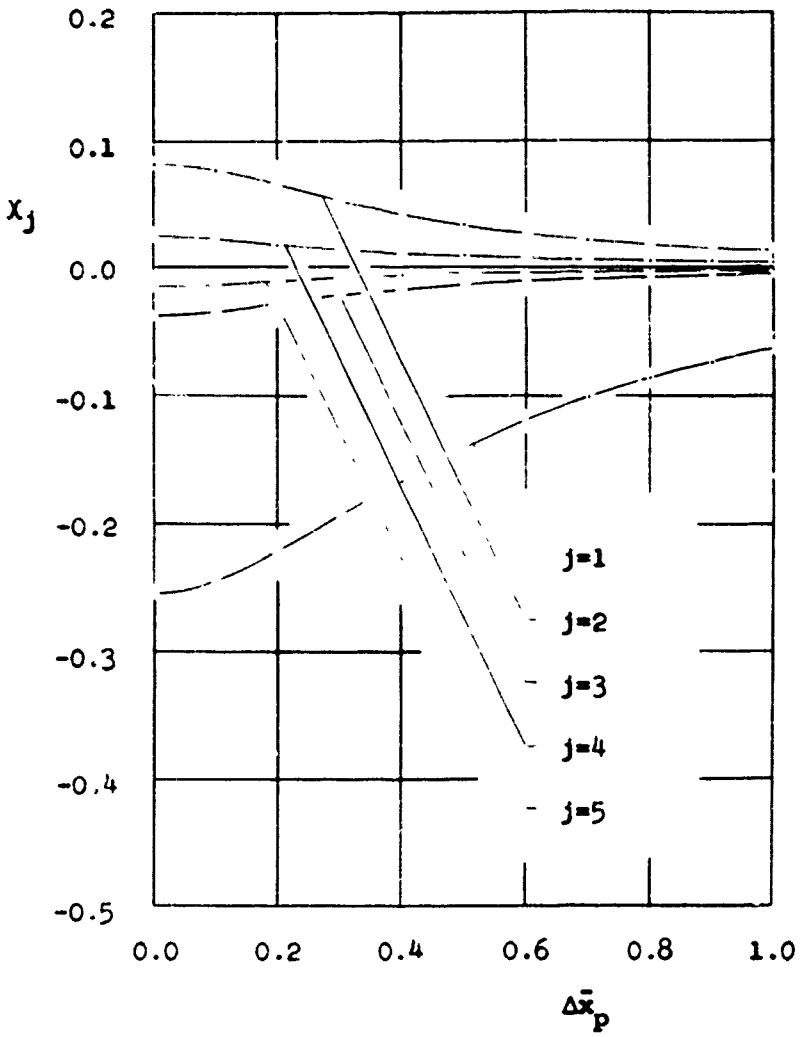

FIGURE 3.2

CHARACTERISTIC FUNCTIONS X_j FOR μ=0.75

TABLE 3.2

CHARACTERISTIC FUNCTIONS X_j FOR $\mu = 0.75$

$\pm\Delta\bar{x}_p$	$-X_1$	X_2	$-X_3$	X_4	$-X_5$
0.00	0.25560	0.08093	0.03917	0.02296	0.01503
0.05	0.25317	0.07963	0.03837	0.02242	0.01466
0.10	0.24639	0.07602	0.03619	0.02098	0.01364
0.15	0.23614	0.07077	0.03309	0.01897	0.01224
0.20	0.22356	0.06464	0.02962	0.01678	0.01075
0.25	0.20972	0.05831	0.02617	0.01467	0.00934
0.30	0.19543	0.05219	0.02299	0.01277	0.00810
0.35	0.18126	0.04654	0.02018	0.01114	0.00705
0.40	0.16758	0.04147	0.01775	0.00976	0.00617
0.45	0.15462	0.03700	0.01569	0.00861	0.00544
0.50	0.14248	0.03308	0.01395	0.00765	0.00483
0.55	0.13121	0.02968	0.01247	0.00684	0.00433
0.60	0.12081	0.02673	0.01121	0.00616	0.00390
0.65	0.11126	0.02416	0.01013	0.00557	0.00353
0.70	0.10249	0.02192	0.00920	0.00507	0.00321
0.75	0.09447	0.01996	0.00840	0.00463	0.00294
0.80	0.08714	0.01824	0.00769	0.00425	0.00270
0.85	0.08044	0.01673	0.00707	0.00391	0.00248
0.90	0.07433	0.01538	0.00652	0.00361	0.00229
0.95	0.06874	0.01418	0.00602	0.00334	0.00212
1.00	0.06363	0.01311	0.00558	0.00310	0.00197

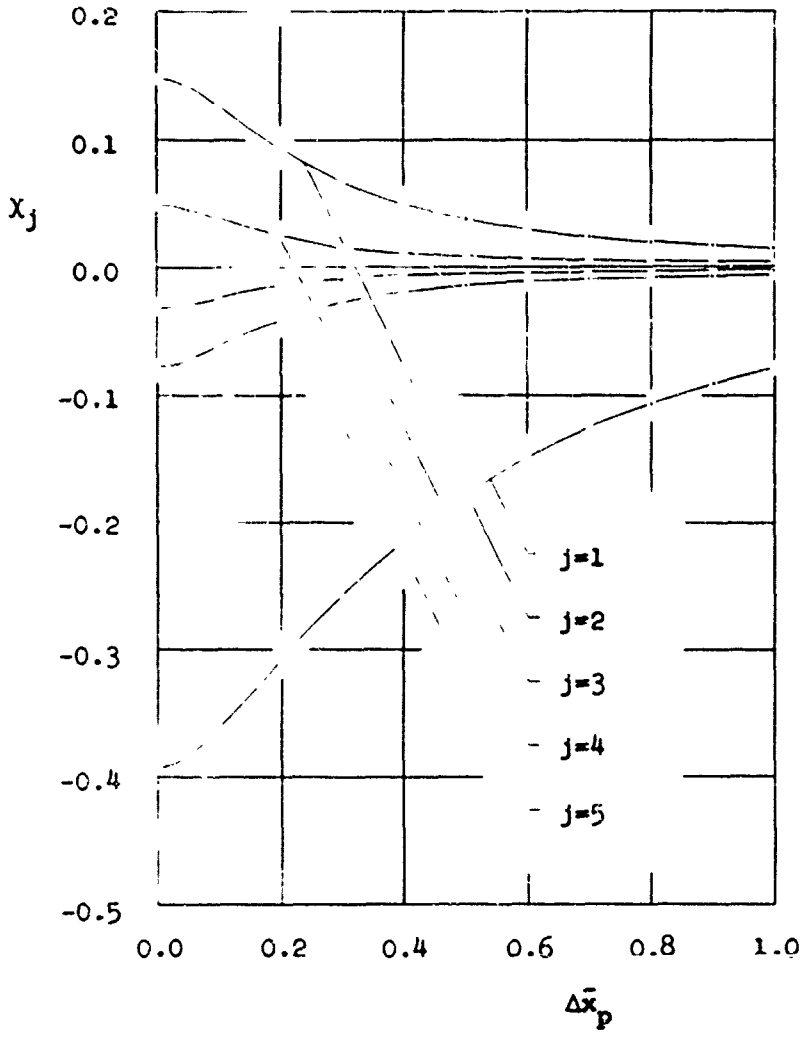

FIGURE 3.3

CHARACTERISTIC FUNCTIONS X_j FOR μ=0.90

TABLE 3.3

CHARACTERISTIC FUNCTIONS X_j FOR $\mu = 0.90$

$\pm\Delta\bar{x}_p$	$-X_1$	X_2	$-X_3$	X_4	$-X_5$
0.00	0.39179	0.14562	0.07773	0.04866	0.03338
0.05	0.38341	0.13947	0.07305	0.04499	0.03044
0.10	0.36257	0.12492	0.06246	0.03701	0.02426
0.15	0.33623	0.10797	0.05100	0.02892	0.01834
0.20	0.30873	0.09194	0.04107	0.02241	0.01386
0.25	0.28215	0.07800	0.03318	0.01760	0.01073
0.30	0.25734	0.06632	0.02713	0.01415	0.00859
0.35	0.23461	0.05671	0.02254	0.01167	0.00710
0.40	0.21396	0.04885	0.01906	0.00988	0.00604
0.45	0.19529	0.04243	0.01639	0.00853	0.00525
0.50	0.17845	0.03716	0.01431	0.00751	0.00465
0.55	0.16328	0.03282	0.01266	0.00670	0.00417
0.60	0.14960	0.02921	0.01133	0.00604	0.00378
0.65	0.13727	0.02620	0.01024	0.00550	0.00345
0.70	0.12612	0.02365	0.00933	0.00504	0.00317
0.75	0.11605	0.02149	0.00855	0.00464	0.00293
0.80	0.10693	0.01962	0.00788	0.00430	0.00272
0.85	0.09865	0.01800	0.00729	0.00399	0.00253
0.90	0.09114	0.01659	0.00678	0.00372	0.00236
0.95	0.08431	0.01535	0.00631	0.00347	0.00220
1.00	0.07809	0.01424	0.00589	0.00325	0.00206

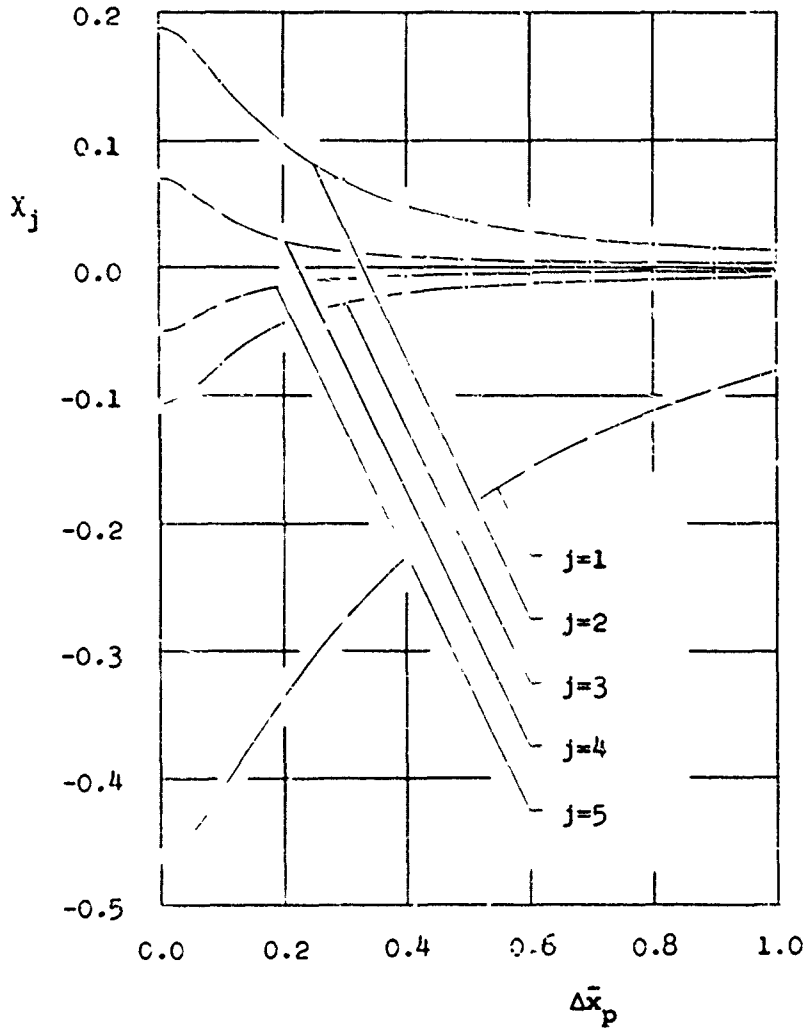

FIGURE 3.4

CHARACTERISTIC FUNCTIONS X_j FOR μ=0.95

TABLE 3.4

CHARACTERISTIC FUNCTIONS χ_j FOR $\mu = 0.95$

$\pm\Delta\bar{x}_p$	$-\chi_1$	χ_2	$-\chi_3$	χ_4	$-\chi_5$
0.00	0.46299	0.18750	0.10654	0.07000	0.04994
0.05	0.44552	0.17310	0.09451	0.05980	0.04120
0.10	0.41050	0.14641	0.07381	0.04347	0.02810
0.15	0.37306	0.12091	0.05605	0.03078	0.01882
0.20	0.33766	0.09956	0.04279	0.02225	0.01314
0.25	0.30543	0.08238	0.03326	0.01669	0.00972
0.30	0.27652	0.06874	0.02647	0.01306	0.00762
0.35	0.25071	0.05795	0.02161	0.01064	0.00628
0.40	0.22773	0.04939	0.01809	0.00898	0.00537
0.45	0.20725	0.04256	0.01548	0.00779	0.00472
0.50	0.18898	0.03707	0.01351	0.00690	0.00423
0.55	0.17264	0.03262	0.01198	0.00621	0.00384
0.60	0.15801	0.02898	0.01076	0.00565	0.00352
0.65	0.14488	0.02596	0.00977	0.00519	0.00325
0.70	0.13307	0.02344	0.00895	0.00480	0.00302
0.75	0.12241	0.02131	0.00825	0.00445	0.00281
0.80	0.11279	0.01948	0.00765	0.00415	0.00262
0.85	0.10408	0.01791	0.00712	0.00388	0.00245
0.90	0.09618	0.01654	0.00664	0.00364	0.00230
0.95	0.08900	0.01533	0.00622	0.00341	0.00216
1.00	0.08247	0.01426	0.00583	0.00321	0.00204

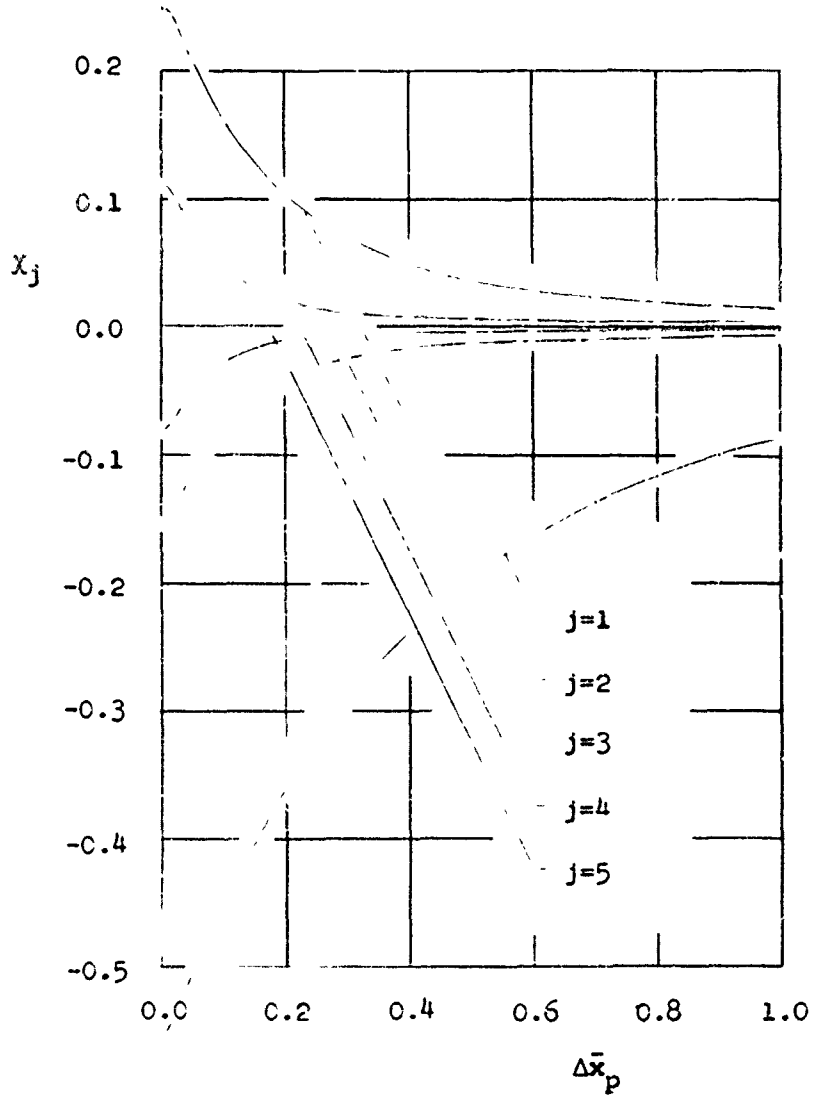

FIGURE 3.5

CHARACTERISTIC FUNCTIONS X_j FOR μ=0.99

TABLE 3.5

CHARACTERISTIC FUNCTIONS χ_j FOR $\mu = 0.99$

$\pm\Delta\bar{x}_p$	$-\chi_1$	χ_2	$-\chi_3$	χ_4	$-\chi_5$
0.00	0.55041	0.24839	0.15401	0.10893	0.08285
0.05	0.50412	0.20640	0.11589	0.07423	0.05118
0.10	0.44968	0.16277	0.08094	0.04614	0.02850
0.15	0.40135	0.12906	0.05748	0.02973	0.01693
0.20	0.35920	0.10346	0.04198	0.02025	0.01105
0.25	0.32248	0.08400	0.03166	0.01468	0.00796
0.30	0.29043	0.06913	0.02471	0.01132	0.00625
0.35	0.26236	0.05769	0.01995	0.00921	0.00523
0.40	0.23768	0.04881	0.01662	0.00783	0.00457
0.45	0.21590	0.04185	0.01423	0.00689	0.00412
0.50	0.19661	0.03633	0.01246	0.00619	0.00376
0.55	0.17945	0.03191	0.01111	0.00565	0.00348
0.60	0.16415	0.02832	0.01005	0.00521	0.00324
0.65	0.15046	0.02538	0.00920	0.00484	0.00303
0.70	0.13818	0.02293	0.00848	0.00452	0.00284
0.75	0.12712	0.02088	0.00788	0.00423	0.00267
0.80	0.11715	0.01913	0.00735	0.00398	0.00251
0.85	0.10813	0.01762	0.00688	0.00374	0.00237
0.90	0.09996	0.01631	0.00646	0.00353	0.00224
0.95	0.09253	0.01516	0.00607	0.00333	0.00211
1.00	0.08578	0.01413	0.00572	0.00315	0.00200

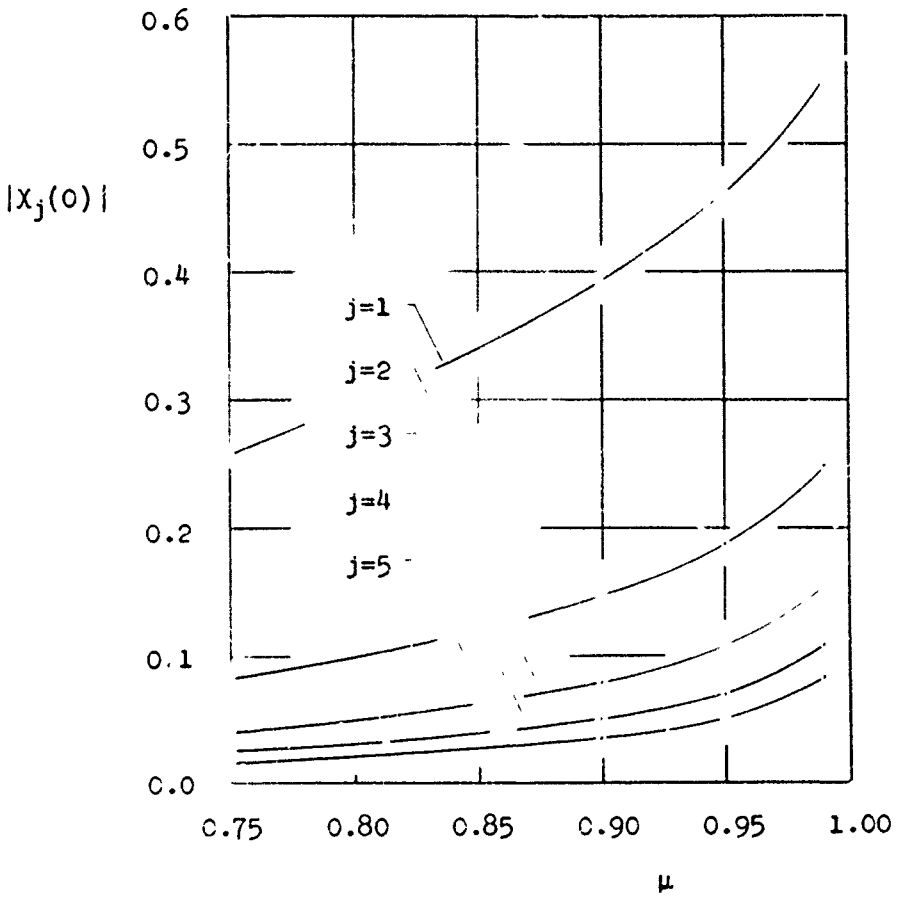

FIGURE 3.6

VARIATION OF CHARACTERISTIC FUNCTION MAXIMUM WITH TIP RATIO PARAMETER

tabulated values of the Legendre function[14,15]. Over a range of values of μ and $\Delta\bar{x}_p$, the results may be estimated from Fig. 2.1. For zero tip clearance, they possess a logarithmic singularity near the propeller plane. Since Eqs. (1.6), (1.18) and (2.8) show that the radial velocity at x_s, R induced by a ring vortex of radius r_v is $-U\Delta\bar{x}_v Q_{\frac{1}{2}}'(\tilde{m}_3)/4\pi R\bar{r}_v^{\frac{1}{2}}$, a perfect differential in $\bar{x}_v$, Eq. (3.8) is equivalent to the effect of a semi-infinite cylindrical distribution of vortex rings of radius R_p, extending from x_p to $+\infty$. The corresponding constant strength per unit length in the axial direction is $UN\Gamma_M\mu/\pi J$, or alternatively, a uniform slipstream velocity increment of the same amount. In this way, the previous results[7] using the method of singularities, i.e., determing the effect of the propeller by a pressure jump and uniform slipstream, can be related to the present analysis by setting $\mu = 1$ and $\bar{x}_p = \lambda$ in Eq. (3.8).

3.3 Limiting Case of Infinite Advance Ratio

As the forward velocity U becomes very large compared to the rotational velocity ΩR_p at the propeller tip, we have shown that the swirl terms disappear from the kernel. This decoupled our governing equations, Eqs. (2.35) and (2.36), for the chordwise shroud vortex distributions and reduced the kernel K_m' to Weissinger's result. In terms of Legendre functions, the reduced kernel is given by the sum of Eqs. (2.9) and (2.37).

Now, if we let the advance ratio become infinite in the "shed" propeller term $C_{\Gamma\acute{m}}$ and follow the derivation of Eq. (2.37), we find that this term is purely imaginary, or

$$\lim_{J \to \infty} C_{\Gamma\acute{m}} =$$

$$- \frac{i\mu N}{8\pi^2} \int_0^{\mu} \frac{\bar{\Gamma}'}{\bar{r}_v^{\frac{1}{2}}} \int_0^{\infty} T'_{mN} \, d\hat{\tau} \, d\bar{r}_v \qquad (3.9)$$

The argument of T'_{mN} is equal to $\tilde{\omega}_4$ with $J\mu\bar{\tau}$ replaced by its equivalent $\hat{\tau}$. From their definitions, then, $B_{\Gamma\acute{m}}$ is identically zero in this case and $A_{\Gamma\acute{m}}$ is given as minus twice the imaginary part of Eq. (3.9). The single "bound" propeller term remains unchanged.

With these results, Eqs. (2.35) and (2.36) are further simplified for an infinite advance ratio. The subsequent shroud vortex distributions for any harmonic can be found from Weissinger's solutions[9] for a ring wing at zero angle of attack in a uniform stream. In particular, for B_m we see that $B_1, B_2, \ldots$ are all zero since the real shroud camber appears only in the zeroth harmonic. The remaining B_C with $B_{\Gamma\acute{C}} = 0$ is the distribution for the actual duct, which is assumed axisymmetric, without the propeller present. This, of course, is the same as noted for B_C for finite J since there are no shed vortices for axisymmetric loading.

On the other hand, for A_m, $A_C \equiv 0$ and $A_1, A_2, \ldots$

correspond to the vortex distributions of an equivalent asymmetric duct under identical flow conditions. The equivalent axially asymmetric camber, say $\epsilon_{J\infty}$, has just a sine harmonic dependence, or,

$$\epsilon_{J\infty} = \sum_{m=1}^{\infty} \epsilon_{Jm}\,(\Delta\bar{x}_p)\,\sin mN\theta_s \tag{3.10}$$

where the axial camber coefficients

$$\epsilon_{Jm} \equiv \lim_{J\to\infty} -2\beta(C_{\Gamma m}+C_{\Gamma\dot{m}}) \tag{3.11}$$

follow directly from Eqs. (2.30) and (3.9). That is:

<u>At high advance ratio, the resultant shroud loading on a ducted propeller at zero angle of attack in a uniform inviscid flow is equal to the load on the isolated shroud plus the loading on an equivalent asymmetric ring wing</u>.

The inner integration on $T'_{mN}(\bar{\omega}_4)$ over $\hat{\tau}$ in Eq. (3.9) is given by Eq. (2.41) for $\bar{r}_v = 1$ and by the infinite series,

$$\int_0^{\infty} T'_{mN}\,d\hat{\tau} = \sum_{j=0}^{\infty} \frac{\Delta\bar{x}_p^{2j+1}}{j!(2\bar{r}_v)^j}\; T_{mN}^{(j+1)} + \frac{\pi\bar{r}_v^{\frac{1}{2}}}{4}\left[\frac{(f^{mN}-f^{-mN})(f^{-1}-f)}{(\bar{\omega}_5^2-1)^{\frac{1}{2}}} - 2\delta_{2,mN}\right] \tag{3.12}$$

for $0 \leq \bar{r}_v < 1$. The argument of the $(j+1)^{th}$ derivative is $\tilde{\omega}_5 \equiv \{1+(1-\bar{r}_v)^2/2\bar{r}_v\}$ or $\tilde{\omega}_3$ of Eq. (2.18) with $\Delta\bar{x}_p = 0$, i.e., the propeller plane, and $f \equiv \{\tilde{\omega}_5-(\tilde{\omega}_5^2-1)^{1/2}\}$. To derive Eq. (3.12), T'_{mN} is re-expressed in the integral form of the Legendre function of Eq. (2.8) and the order of integration is interchanged. The integration on τ , which represents the influence of a straight semi-infinite vortex, can then be performed. Expanding part of the subsequent integrand over θ in reciprocal square-root powers of $\{(1-\bar{r}_v)^2+4\bar{r}_v \sin^2\theta\}$, the integral of each term is identified from Eq. (2.8) as a derivative of a Legendre function of second kind and half order. The other part is evaluated by suitable contour integration.

3.4 Infinite Blade Number

In many instances, the propeller blade number may become quite large. For this case, an actuator disk solution is desired which is the proper limit of our equations, retaining the radial propeller load variation.

The propeller disk loading is proportional to the product of the blade number and the strength of the blade circulation. To obtain an actuator disk solution, we let the blade number approach infinity but decrease the strength of the circulation such that the product remains finite, or

$$\bar{\Gamma}_M \equiv \lim_{N \to \infty,\ \Gamma_M \to 0} N\Gamma_M \qquad (3.13)$$

If we examine the propeller modification of the shroud camber by the zeroth harmonic, see Eq. (3.6), we find that for these parameters its only dependence is linear with their product. In the limit, then, this camber modification persists unchanged and equal to the finite blade result.

On the other hand, the frequency of the first harmonic and other time dependent terms of the shroud loading becomes infinite. By definition of any actuator disk model, however, the flow field must be time independent in coordinates translating with the propeller. Since these higher harmonics are purely sinusoidal, their amplitude for infinite blade number and finite disk loading must approach zero. Physically, this establishes that:

<u>The average pressure distribution on the shroud of a ducted propeller with a finite blade number corresponds to the total loading on a similar model with an infinite blade number but the same disk loading</u>.

For an analytic proof, we have to note that the parameters m,N, and Γ_M occur in the propeller terms, see Eqs. (2.29) (2.30) and (2.31), only as the product mN and $N\Gamma_M$. The kernels, of course, contain just mN as a parameter. Mathematically, then, we have to expand $Q_{n-\frac{1}{2}}$ for large order near its singularity to show that all the propeller terms except $B_{\Gamma 0}$ vanish and that the integral equations decouple.

The zeroth harmonic of the propeller terms for the actuator disk limit has a broader significance. The term $B_{\Gamma 0}$

gives the radial velocity component of a generalized actuator disk. The computation of the axial and tangential velocity components is analogous to that of B_{r0} . This model is not limited to a uniform disk loading, nor to zero angle of attack if the slipstream deflection is known. In other words:

The steady part of the flow field of any propeller with finite blade number corresponds to the generalized actuator disk solution with the same disk loading.

3.5 General Solution for Higher Harmonics

We have shown that the higher harmonics, $m = 1,2,3 \ldots$, correspond to the time-dependent terms of the shroud loading. The governing equations have, in general, two essential features which make a numerical solution more complex than the ring wing problem. One is the coupling, and the other, the occurrence of a logarithmic as well as a Cauchy singularity. These difficulties can be treated by modification of Weissinger's technique, but further reduction is more desirable.

First, it is possible to remove the coupling because of the "derivative" relationship between the kernels. For $m \geq 1$, we let

$$I_A \equiv \int_{-\lambda}^{\lambda} A_m(\bar{x}_v)\, K_m(\Delta\bar{x}_v)\, d\bar{x}_v$$

$$I_B \equiv \int_{-\lambda}^{\lambda} B_m(\bar{x}_v)\, K_m(\Delta\bar{x}_v)\, d\bar{x}_v \qquad (3.14)$$

and note

$$K_m'(\Delta\bar{x}_v) \quad \frac{d}{d\bar{x}_s} \quad K_m(\Delta\bar{x}_v) \tag{3.15}$$

With Eqs. (3.14) and (3.15), Eqs. (2.35) and (2.36) become a system of linear differential equations. Or, without the shroud camber,

$$\sigma I_A - I_B' = - B_{\Gamma m}$$

$$\sigma I_B + I_A' = A_{\Gamma m} + A_{\Gamma m'} \tag{3.16}$$

where differentiation across the integrals I_A and I_B is justified in view of the weak square-root and logarithmic singularities of the integrands. Multiplying the first of Eqs. (3.16) by $\sigma \equiv mN/J\mu$ and adding it to the derivative of the second, we isolate I_A; reversing the procedure and subtracting, I_B. Both are of the form

$$I'' + \sigma^2 I = P(\bar{x}_s) \tag{3.17}$$

which is the second-order, linear differential equation for a simple harmonic oscillator subject to a forcing function. That is, we view the integrals I_A and I_B of our unknown vortex distributions as "particle displacement" and the axial coordinate $\bar{x}_s$ as "time". The "motion" is undamped with a

"natural frequency" σ . The "forcing functions" for I_A and I_B are,

$$P_A = (A_{\Gamma m}+A_{\Gamma m'})' - \sigma B_{\Gamma m'}$$

$$P_B = (B_{\Gamma m'})' + \sigma(A_{\Gamma m}+A_{\Gamma m'}) \qquad (3.18)$$

respectively.

From these differential equations, I_A and I_B are determined, providing in turn, decoupled equations for A_m and B_m . To find the <u>inhomogeneous solution</u> I_i of Eq. (3.17), we take the "indicial response" I_u of the system to the unit step function $P = 1(\bar{x}_s)$,

$$I_u = (1/\sigma^2)(1-\cos \sigma\bar{x}_s)\, 1(\bar{x}_s) \qquad (3.19)$$

and use Duhamel's[24] linear superposition method. After integration by parts, we have

$$I_i = \frac{1}{\sigma} \int_{-\lambda}^{\bar{x}_s} P(\bar{x}) \sin \sigma(\bar{x}_s-\bar{x})\, d\bar{x} \qquad (3.20)$$

where P we know is well-behaved throughout the interval from $-\lambda$ to λ for $0 \leq \mu < 1$.

Eq. (3.20), together with Eqs. (3.14) and (3.18), yield a simpler system of decoupled equations for the time-dependent shroud vortex distributions which correspond to the first and

higher harmonics of the radial flow induced by the propeller. The form of these equations is similar to the general ring wing problem, but the kernel is completely different. However, if we differentiate with respect to $\bar{x}_s$, carry the differentiation back inside I_A and I_B, and use Eq. (3.15), we find for the inhomogeneous solution,

$$\int_{-\lambda}^{\bar{x}_s} P_A(\bar{x}) \cos \sigma \Delta\bar{x} \, d\bar{x}$$

$$\int_{-\lambda}^{\lambda} A_m(\bar{x}_v) \, K_m'(\Delta\bar{x}_v) \, d\bar{x}_v \qquad (3.21)$$

and,

$$\int_{-\lambda}^{\bar{x}_s} P_B(\bar{x}) \cos \sigma \Delta\bar{x} \, d\bar{x}$$

$$\int_{-\lambda}^{\lambda} B_m(\bar{x}_v) \, K_m'(\Delta\bar{x}_v) \, d\bar{x}_v \qquad (3.22)$$

where the "bound" term of K_m', or $-S_{mN}'/4\pi$, is the same as for the ring wing. Numerical solutions, then, can follow essentially along the lines of Weissinger's[9].

The decoupling technique which we have employed raises an important question. In addition to the inhomogeneous

solution of the differential equation of Eq. (3.17), there is the homogeneous solution I_h ,

$$I_h(\bar{x}_s) = I_h' \cos \sigma \Delta\bar{x}' + (1/\sigma)\, I_h'' \sin \sigma \Delta\bar{x}' \qquad (3.23)$$

where I_h' denotes the value of $I_h(\bar{x}_s)$ at any reference point between the leading and trailing edges with the leading edge excluded; and $\Delta\bar{x}'$, the distance from the reference point to $\bar{x}_s$. These solutions introduce a total of four unknown constants for the corresponding I_A and I_B . Two of these, though, result from the differentiation required for decoupling. They may be removed by resubstitution into either of Eqs. (3.16) , which shows that the relations,

$$\sigma I_{hA} - I'_{hB} = C$$

$$\sigma I_{hB} + I'_{hA} = C \qquad (3.24)$$

must be fulfilled in order for the coupled, homogeneous equations to be satisfied. We are thus left with two undetermined constants as we should expect.

That is, consider an <u>axisymmetric ring wing</u> at zero incidence in a uniform, translating and rotating flow, with the axis of rotation coincident with the wing axis. The equations

seem to indicate, then, that it is possible in an inviscid fluid to have self-sustaining load distributions of periodic nature. Or, the radial velocity induced by the helical vortices shed from the shroud for certain shroud vortex distributions balances the velocity induced by the bound shroud vortices. This is independent of the camber within the present assumptions, but dependent on the swirl, vanishing as the shroud "advance ratio" becomes infinite and decouples the governing equations. The possible existence of these self-sustaining solutions appears to be similar in nature to the recent investigation of H. Ludwieg[10], where he has examined the "stability against the formation of helical vortices" in an annular flow between two coaxial cylinders.

3.6 Example

To illustrate the practical application of the theory we have computed the average shroud load distribution for a particular ducted propeller.

The values used for the parameters and the propeller loading assumed are,

$$J = 1$$

$$N = 2$$

$$\bar{x}_p = 0$$

$$\epsilon = -0.38\ \bar{x}$$

$$\bar{\Gamma} = (2/3\sqrt{3})(2 \sin \pi\hat{r} - \sin 2\pi \hat{r})$$

$$\lambda = 0.5$$

$$\mu = 0.95 \qquad (3.25)$$

where $\bar{\Gamma}$ is shown in Fig. 3.7.

With $\Gamma_1 = 4/3\sqrt{3}$, $\Gamma_2 = -2/3\sqrt{3}$ and $\Gamma_M = 1$, we have computed and plotted in Fig. 3.8 the propeller contribution, $-B_{\Gamma,0}/2$, to the effective camber by means of Eq. (3.6) and Table 3.4. The maximum camber distortion which occurs at the mid chord or propeller plane is about 40% of the given shroud camber at the trailing edge. The assumed $\bar{\Gamma}$ corresponds to a disk loading, neglecting inflow, of 41.1 psf at U = 200 mph and STP.

From Eq. (2.44), the net average pressure distribution $\Delta\bar{p}]$ becomes by means of Eqs. (2.1) and (2.2),

$$\bar{c}_{p]} = -B_0(\bar{x}) \qquad (3.26)$$

where $\bar{c}_{p]} \equiv \Delta\bar{p}]/(\rho U^2/2)$. For the determination of $B_0(\bar{x})$ for our example, we have employed an iteration technique[25] instead of Weissinger's procedure for the solution of Eq. (3.1). The final result is shown in Fig. 3.9. It required eleven non-zero terms, including the singular term, of the Glauert series and two iterations to obtain accuracy to three decimal places.

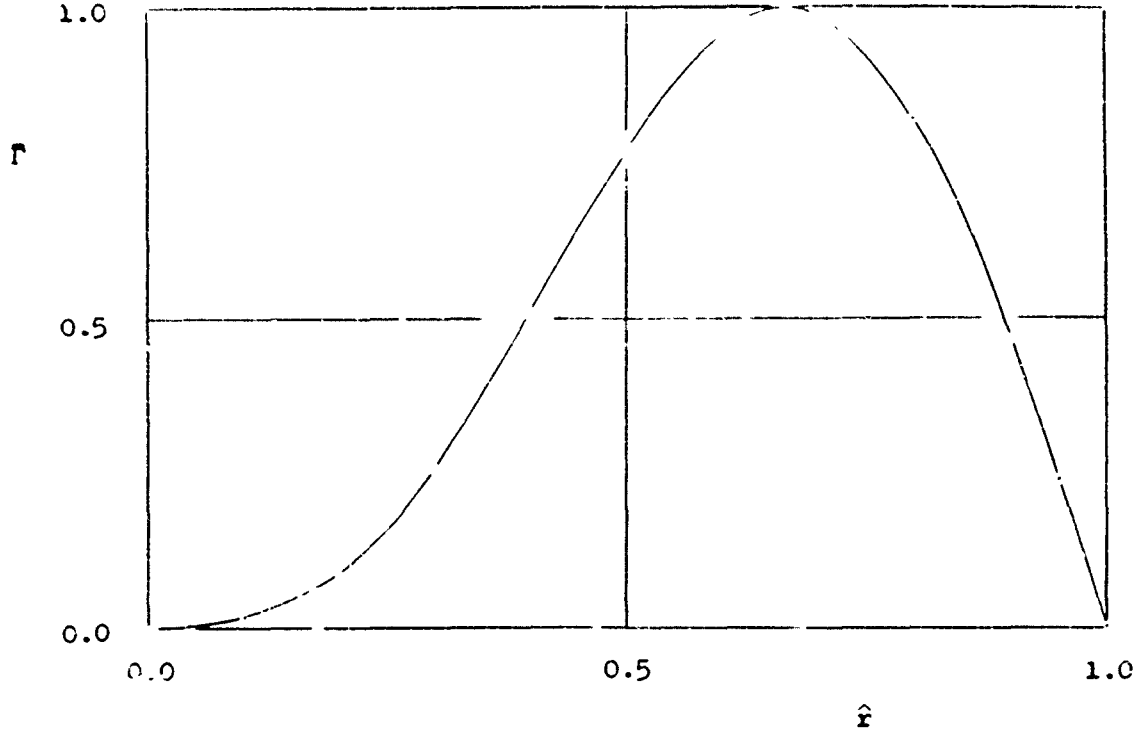

FIGURE 3.7

BLADE CIRCULATION DISTRIBUTION FOR EXAMPLE

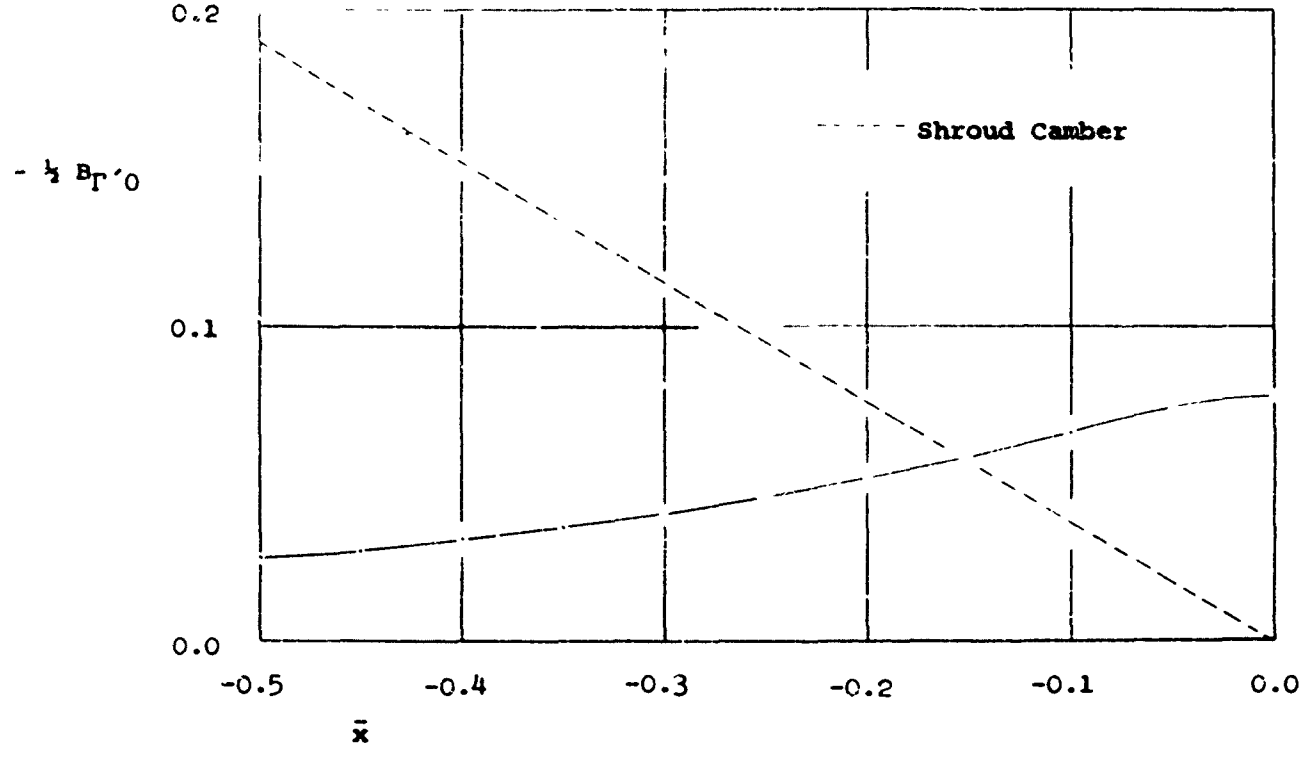

FIGURE 3.8

PROPELLER CONTRIBUTION TO EFFECTIVE SHROUD CAMBER FOR EXAMPLE

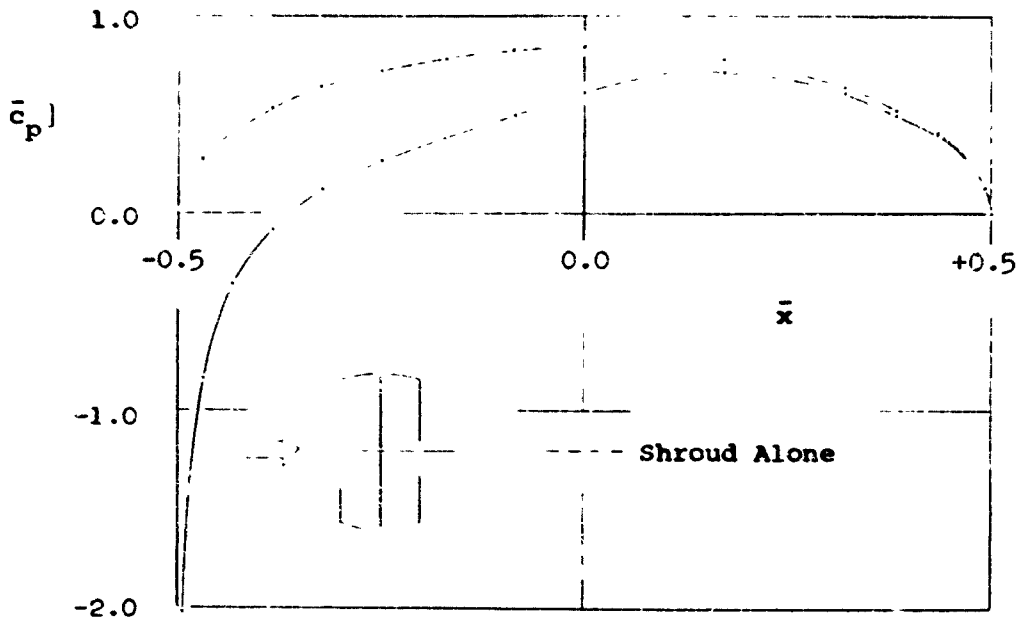

FIGURE 3.9

NET STEADY PRESSURE DISTRIBUTION ON THE SHROUD FOR EXAMPLE

$\epsilon=-0.36\bar{x}$, N=2, J=1, $\bar{x}_p=0$, $\mu=0.95$, $\lambda=0.5$

$\Gamma_M=1$, $\Gamma_1=4/3\sqrt{3}$, $\Gamma_2=-2/3\sqrt{3}$, Γ_3 ... $=0$

Without the propeller, the net loading is symmetric about the center of the shroud and vanishes at the leading and trailing edges because the camber is antisymmetric. The contribution of the propeller, however, is always symmetric and so in this case introduces flow around the leading edge and a leading edge singularity. This, in turn, gives rise to a leading edge suction force which can be found from the value of 0.187 for the coefficient of the singular term of B_0 .

CONCLUSIONS

A three-dimensional theory has been developed for the ducted propeller with finite blade number in uniform motion through an inviscid, incompressible fluid at zero incidence. Within the approximations of a lightly-loaded propeller and of thin airfoil theory, the following generalizations were obtained:

> The effect of shroud camber appears only in the steady shroud load.
>
> The steady pressure difference across the shroud is identical to that of a similar ring wing of different camber.
>
> At high advance ratio, the resultant shroud loading is equal to the load on the isolated shroud plus the loading on an equivalent asymmetric ring wing.
>
> The steady pressure distribution on the shroud corresponds to the total loading on a similar configuration with infinite blade number but the same radial disk loading.
>
> The steady part of the flow field of any propeller with finite blade number corresponds to a generalized actuator disk solution with the same radial disk loading.

The theory is readily applicable to practical calculations, particularly the determination of the zeroth harmonic which gives the average shroud loading. By variation of parameters, the optimum configurations of Dickmann and Weissinger[7] and R. B. Gray and W. Castles, Jr.[26] may be further investigated.

These results clearly justify similar analytic studies of the more complex ducted propeller problems.

REFERENCES

1. Stipa, L., Experiments with Intubed Propellers, L'Aerotecnica, pp. 923-953, August 1931, (Translated by Dwight M. Miner, NACA, NACA TM 655, January 1932).

2. Kort, L., Der neue Düsenschrauben-Antrieb, Werft-Reederei-Hafen, Jahrgang 15, Heft 4, February 15, 1934. (Obtained from Stanford University Library).

3. Sacks, A. H. and Burnell, J., Ducted Propellers - A Critical Review of the State of the Art, ARD-232, Miller Aircraft Corporation, June 26, 1959.

4. Meyerhoff, L. and Finkelstein, S. B., On Theories of the Duct Shape for a Ducted Propeller, PIBAL Report No. 164, Polytechnic Institute of Brooklyn, August 1958.

5. Megrue, J., A Brief Survey of Ducted Propeller Literature, TAR-MEMO 592, Therm Advanced Research, November 1959.

6. Küchemann, D. and Weber, J., Aerodynamics of Propulsion, Chapter 6 - The Ducted Propeller. First Edition, McGraw-Hill Book Company, Inc., New York, 1956.

7. Dickmann, H. E., Weissinger, J., Beitrag zur Theorie optimaler Düsenschrauben (Kortdüsen), Jahrbuch der Schiffbautechnischen Gesellschaft, Band 49, 1955.

8. Lerbs, H. W., Theoretical Considerations on Shrouded Propellers, Navy Department, David Taylor Model Basin, Report C-543, June 1953.

9. Weissinger, J., Einige Ergebnisse aus der Theorie des Ringflügels in Inkompressibler Strömung, Advances in Aeronautical Sciences, Vol. 2, Pergamon Press, 1959, pp. 798-831.

10. Ludwieg, H., Stabilität der Strömung in einem zylindrischen Ringraum, ZFW, Heft 5, Mai 1960, pp. 135-140.

11. Moriya, T., Selected Scientific and Technical Papers, The Moriya Memorial Committee, Department of Aeronautics, University of Tokyo, August 1959.

12. Weissinger, J., Zür Aerodynamik der Ringflügels in inkompressibler Strömung, ZFW, Heft 3/4, März/April 1956, pp. 141-150.

13. Sonnerup, B. O. U., Expression as a Legendre Function of an Elliptic Integral Occurring in Wing Theory, TAR-TN 59-1, Therm Advanced Research, November 1960.

14. Briggs, L. J. and Lowan, A. N., Tables of Associated Legendre Functions, Columbia University Press, 1945.

15. Sluyter, M. M., A Computational Program and Extended Tabulation of Legendre Functions of Second Kind and Half Order, TAR-TR 601, Therm Advanced Research, August 1960.

16. Tsakonas, S. and Breslin, J., Marine Propeller Pressure Field Including Effects of Loading and Thickness, Trans. Soc. Nav. Mar. Engrs. 67, 1959.

17. Riegels, F., Formeln und Tabellen für ein in der räumlichen Potentialtheorie auftretendes elliptisches Integral, Archiv der Mathematik 2, 1949-50, p. 117.

18. Drzewiecki, S., Théorie générale de l'Hélice, Paris, 1920.

19. Ladurner, O., Theoretical Investigation and Examination by Measuring Tests in What a Degree the Economy of Flying Vehicles is Influenced by Pre-cambered Skeletons of Airfoils Closed in Themselves, Bureau Technique Zborowski, DA-91-508-EUC-393, August 1959.

20. Malavard, L. C., Recent Developments in the Method of the Rheoelectric Analogy Applied to Aerodynamics, JAS, May 1957, Vol. 24, pp. 321-331.

21. Weissinger, J., The Influence of Profile Thickness on Ring Airfoils in Steady Incompressible Flow, AFOSR TR 57-8, Part II, January 1957.

22. Bagley, J. A., Kirby, N. B. and Mercer, P. J., A Method of Calculating the Velocity Distribution on Annular Aerofoils in Incompressible Flow, RAE TN No. Aero 2571, June 1958.

23. Moran, J. P., Tip Load Distribution of a Ducted Propeller. To be published, Therm Advanced Research.

24. von Kármán, Th., and Biot, M. A., Mathematical Methods in Engineering, McGraw-Hill Book Company, Inc. New York, 1940.

25. Gray, D. E. and Greenberg, M., Higher Harmonic Solutions for the Ducted Propeller. To be published, Therm Advanced Research.

26. Gray, D. E. and Castles, Jr., W. An Investigation of An Approach to the Problem of Determing the Optimum Design of Shrouded Propellers, Eng. Exp. Station, Georgia Institute of Technology Project No. 9R 38-01-017. Rept. TAEC 60-44, May 1960.